Dalton Transactions

ROYAL SOCIETY OF CHEMISTRY

PAPER

View Article Online
View Journal | View Issue

Cite this: *Dalton Trans.*, 2025, **54**, 15561

Mixed ligand Cu(II) complexes as new precursors for the synthesis of CuO nanomaterials: development of homogeneous and heterogeneous catalysts for styrene epoxidation and phenol hydroxylation under mild conditions

Mitu Sharma, *†[a] Mukesh Sharma, ‡[a] Sazida Yasmin Sultana, [a] Mallayan Palaniandavar *[b] and Nashreen S. Islam *[a]

A new synthetic strategy for obtaining CuO nanocatalysts has been devised using a pair of newly synthesized mixed ligand Cu(II) complexes as the precursors. The new Cu(II) complexes are of the types [Cu(def)(bpy)(NO_3)] **1** and [Cu(def)(phen)(H_2O)]NO_3·(CH_3OH) **2**, where def (deferiprone) is the primary ligand and bpy (2,2′-bipyridine) and phen (1,10-phenanthroline) are the co-ligands. They have been employed as the synthetic precursors for the straightforward synthesis of CuO nanomaterials. The single crystal X-ray structures of **1** and **2** reveal that both the complexes possess square pyramidal coordination geometries. The mixed ligand-templated CuO nanomaterials **3** and **4** have been obtained *via* thermal degradation of the complexes **1** and **2**, respectively. They have been comprehensively characterized using FT-IR, UV-DRS, XRD, SEM, TEM, and BET analyses. The CuO nanocomposites have been found to be efficient heterogeneous catalysts for the selective styrene epoxidation with H_2O_2, yielding a striking 99.7% conversion and 99.3% selectivity under organic solvent-free conditions. Also, the same nanocatalysts displayed remarkable efficiency as water tolerant heterogeneous catalysts to facilitate phenol hydroxylation (65.9/67.8% conversion) with H_2O_2 in aqueous medium. They could be easily recovered and recycled for at least three consecutive cycles without significant lowering of their selectivity or activity profile. The precursor mixed ligand complexes **1** and **2**, on the other hand, served as homogeneous catalysts in the epoxidation of styrene under similar solvent-free reaction conditions with 98.5/97.3% conversion and around 99% selectivity, as well as in the phenol hydroxylation in aqueous medium with 63.2/69.3% conversion.

Received 16th June 2025,
Accepted 16th September 2025

DOI: 10.1039/d5dt01420d

rsc.li/dalton

1. Introduction

Copper oxide (CuO) nanostructures have been receiving a great deal of contemporary attention over the past two decades, as they constitute a fascinating class of low-cost nanomaterials[1,2] with applications in diverse areas ranging from gas sensors,[3] electrode materials,[4,5] Li/K ion batteries,[6] contrast agents for MRI,[7] anticancer[8,9] and antimicrobial agents[10] to catalysts.[11,12] Accordingly, much of the recent work has been focused on developing viable procedures for the controlled synthesis of CuO nanomaterials with different morphologies and particle size and screening them for various activities.[13] However, most of the reported synthetic methodologies for obtaining CuO nanoparticles (NPs) require costly templating agents, surfactants, or capping agents for their stability.[14] Also, their synthesis requires tedious trial-and-error processes that often lead to waste.[15] In this context, the use of appropriate Cu(II) complexes as synthetic precursors to derive CuO NPs appears to be a promising greener alternative pathway. For instance, recently, Zhang *et al.* reported the development of copper-based composites using the di-copper(II)-tetrapyridyl ligand complex as the synthetic precursor.[16] However, so far, there appears to be very little exploration of the utility of soluble Cu(II) complexes as precursors for preparing CuO NPs.[16–20]

The CuO NPs have been reported to exhibit excellent activity in catalytic oxidation of a variety of organic substrates like alkenes, alcohols, and aldehydes.[21–23] Among the multitude of organic oxidations, olefin epoxidation and hydroxylation of phenol (PH) to catechol (CT) and hydroquinone (HQ) are primar-

[a]*Department of Chemical Sciences, Tezpur University, Tezpur 784 028, India. E-mail: mitusharma3@gmail.com, nashreen.islam@rediffmail.com*
[b]*School of Chemistry, Bharathidasan University, Tiruchirappalli 620 024, Tamil Nadu, India. E-mail: palanim51@yahoo.com*
†Present address: Department of Chemistry, Brookhaven National Laboratory, Upton, New York 11973-5000, USA.
‡Present address: Department of Chemistry, Suren Das College (Autonomous), Hajo, Kamrup 781102, Assam, India.

ily important for many industrial organic synthesis processes. Epoxides as well as the phenolic products CT and HQ are generally considered as precious building blocks or synthetic precursors in the preparation of a variety of fine and bulk chemicals. Moreover, the conversion of phenol into value-added products is of great importance from an ecological perspective as well due to the identification of phenol as a hazardous organic pollutant and poorly biodegradable industrial waste.

To date, a multitude of innovative and promising transition metal based catalytic processes have been developed for alkene epoxidation.[24,25] Nevertheless, many of the highly efficient catalytic epoxidation procedures typically utilize costly, non-aqueous organo-hydroperoxides such as *tert*-butyl hydroperoxide (TBHP) as the oxygen source along with volatile organic solvents as well as harsh reaction conditions to attain high activity.[26,27] In this regard, aqueous hydrogen peroxide with its high oxygen content offers a predominantly desirable choice of green oxidant as it is easily available, inexpensive, safe, and generates only water as the by-product.[26] In view of the current intense search for new oxidation methodologies that are not only efficient, selective, and high-yielding, but are also ecologically benign, the use of safer oxidants and organic solvent-free conditions is emerging as a key issue in green synthetic strategies. Organic solvent-free transformations with the potential to contribute considerably to waste minimization[28] are considered economically and industrially useful as well as environmentally safer. In the recent past, our research group has developed various homogeneous and heterogeneous d^0 transition metal compounds that display excellent ability to catalyze H_2O_2-induced oxidations of a range of organic materials including olefins and phenol under organic solvent-free conditions[28,29] or employing natural green solvent water as reaction medium.[30–33] However, reports on water-based copper-catalyzed olefin epoxidation or phenol hydroxylation processes are still limited.[34,35] Moreover, we have found only two reports on solvent-free epoxidation based on homogeneous and heterogeneous Cu catalysts.[24,36]

Motivated by the aforementioned observations, we consider it worthwhile to synthesize new mixed-ligand Cu(II) complexes and to explore the scope of establishing a facile route for transforming the complexes obtained into CuO nanomaterials. One of our major objectives has been to develop efficient and versatile homogeneous and heterogeneous catalytic systems for mild organic oxidations based on the Cu(II) complexes and the corresponding CuO nanomaterials, keeping in view these dual goals. In the present work, we have isolated two new molecular Cu(II) complexes containing the O,O donor ligand deferiprone, and N,N-donor diimine ligands 2,2′-bipyridine and 1,10-phenanthroline. The deferiprone is well known due to its clinical significance as a Fe-chelating ligand.[29,37] It acts also as an excellent ligand due to its high binding affinity towards several metals such as V, Zn, Cu, Al, Ga, *etc*.[29,37–40] However, the catalytic ability of deferiprone-based compounds in organic oxidation reactions has rarely been investigated.[29,39,41,42]

We describe herein the synthesis and structural characterization of heretofore unreported mixed ligand Cu(II) complexes [Cu(def)(bpy)(NO_3)] **1** and [Cu(def)(phen)(H_2O)]NO_3·(CH_3OH) **2**, and their facile transformation leading to the synthesis of CuO nanomaterials. The complexes **1** and **2** as well as the CuO nanomaterials display excellent efficiency as catalysts for the selective styrene epoxidation with H_2O_2 under organic solvent-free conditions and phenol hydroxylation as well under aqueous conditions. The findings of our investigation further demonstrate that the CuO nanocatalysts are stable enough to afford good recyclability for multiple cycles of epoxidation with no significant alteration in the activity/selectivity profile. This appears to be the first report on the catalytic application of a CuO NP system in styrene epoxidation carried out using H_2O_2 under organic solvent free conditions.

2. Experimental section

2.1 Materials and methods

The details regarding materials used for compound synthesis and their sources, and methods employed for compound characterization are described in Text S1.

2.2 Synthesis of copper(II) complexes and CuO NPs

2.2.1 Synthesis of [Cu(def)(bpy)(NO_3)] (1). The complex **1** was prepared by adding copper(II) nitrate trihydrate (0.24 g, 1 mmol) in 5 mL methanol dropwise to a methanolic solution (5 mL) of deferiprone (0.14 g, 1 mmol). The reaction mixture was then stirred for 1 h at room temperature and a clear green solution was obtained which was followed by the addition of the secondary ligand, 2,2′-bipyridine (0.16 g, 1 mmol). The resulting solution was refluxed for 2 h and the dark green solution thus obtained was left for slow evaporation (Scheme 1). Green colored single-crystals suitable for X-ray analysis were obtained after 2 days. The crystals were filtered off, washed with small amounts of cold methanol and stored in airtight containers. Anal. calc. for [Cu(def)(bpy)(NO_3)]: C, 48.62; H, 3.84; N, 13.34; Cu, 15.13; found: C, 48.51; H, 3.89; N, 13.15; Cu, 15.05. FT-IR (KBr pellet, cm^{-1}): ν = 478 (ν(Cu–O)), 534 (ν(Cu–N)) and 1384 ($\nu(NO_3)$); 1600, ν(C═N), weak; 1640, ν(C═O), medium. λ_{max}/nm, in CH_3OH (ε_{max}/M^{-1} cm^{-1}): 633 (50), 309 (24 070), 299 (24 530), 226 (43 930), 202 (60 470). HR-MS (CH_3OH) displays a peak at m/z 357.0833 for [Cu(def)(bpy)]$^+$ species (calc. 357.05).

2.2.2 Synthesis of [Cu(def)(phen)(H_2O)]NO_3·(CH_3OH) (2). The complex **2** was prepared using a similar procedure to that used for the synthesis of **1** but by using the ligand 1,10-phenanthroline (0.19 g, 1 mmol) instead of 2,2′-bipyridine. Upon slow evaporation, dark green crystals were obtained after 2

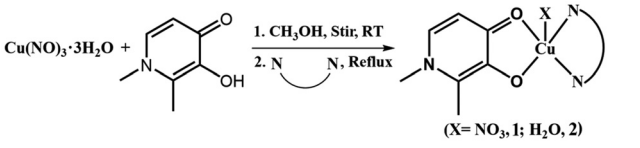

Scheme 1 Schematic representation of the synthesis of complexes **1** and **2**.

days (Scheme 1). Suitable single crystals were selected for X-ray diffraction analysis. Anal. calc. for [Cu(def)(phen)(H_2O)]NO_3: C, 49.41; H, 3.92; N, 12.13; Cu, 13.76; found: C, 49.36; H, 3.48; N, 12.42; Cu, 13.58. FT-IR (KBr pellet, cm^{-1}): ν = 481 (ν(Cu–O)), 579 (ν(Cu–N)), 1384 ($\nu(NO_3)$); 1600, ν(C=N), weak; 1640, ν(C=O), medium and 3392 ($\nu(H_2O)$). λ_{max}/nm, in CH_3OH (ε_{max}/M^{-1} cm^{-1}): 635 (30), 293 (16 070), 271 (33 730), 227 (50 000), 202 (53 930). HR-MS (CH_3OH) displays a peak at m/z 381.1666 for [Cu(def)(phen)]$^+$ species (calc. 381.05).

2.2.3 Synthesis of CuO NPs 3 and 4 using complexes 1 and 2 as precursors. The synthesis of NPs has been achieved by the thermal degradation of the complexes **1** and **2**. In a 20 mL porcelain crucible, 0.50 g of the solid complex **1** was heated at 270 °C for 2 h in the presence of air. After the completion of the process, CuO NPs **3** were obtained as a black residue, which was then washed 8–10 times with deionized water and ethanol under centrifugation and then dried *in vacuo*. The same procedure was then repeated with complex **2** to obtain the CuO NPs **4** (Scheme 2).

2.3. X-Ray crystallography

The molecular structures of compounds **1** and **2** were determined using a Bruker SMART APEX II single crystal X-ray CCD diffractometer at ambient temperature using graphite-monochromatized Mo-Kα radiation (λ = 0.71073 Å). The data were resolved with SHELXS-97 and refined using SHELXL-2014.[43] The graphics interface package used was PLATON and the diagrams were generated using the ORTEP 3.07 generation package.[44] Straight methods were used to obtain the locations of all the atoms and E-maps were used for the positioning of metal atoms of the complexes and the non-hydrogen atoms were refined anisotropically. The hydrogen atoms attached to the carbon atoms were first located in geometrically controlled positions and then refined with isotropic temperature factors ($1.2U_{eq}$ of their parent atoms).

2.4 General procedure for the oxidation of styrene and phenol

2.4.1 Styrene epoxidation. To a reaction mixture of 0.002 mmol of the homogeneous catalyst [**1** (0.83 mg) or **2** (0.98 mg)] or heterogeneous catalyst [**3** (1 mg) or **4** (1 mg)] and styrene (0.2 g, 2.0 mmol), 30% H_2O_2 (0.90 mL, 8 mmol) was added under continuous stirring at 80 °C. The progress of the reaction was monitored by HPLC. After the completion of the reaction, the heterogeneous catalyst [**3** (0.95 mg) or **4** (0.93 mg)] was separated by filtering the reaction mixture and the residue was washed with acetone for further use.

2.4.2 Phenol hydroxylation. In a typical procedure, the oxidation reaction was carried out by placing 0.02 mmol of homogeneous catalyst [**1** (8.3 mg) or **2** (9.8 mg)] or heterogeneous catalyst [**3** (10 mg) or **4** (10 mg)] in water (3 mL) in a round bottom flask. Phenol (0.4705 g, 5 mmol) was then added, followed by the dropwise addition of 30% H_2O_2 (2.26 mL, 20 mmol) under continuous stirring at 80 °C. The progress of the reaction was monitored by HPLC. After the completion of the reaction, the heterogeneous catalyst [**3** (9.3 mg) or **4** (9.7 mg)] was separated by filtering the reaction mixture and washed with water and ethyl acetate for further use.

The quantitative analysis of styrene and phenol and its oxidation products was performed on a Thermo-Scientific Dionex Ultimate 3000 HPLC system attached to a UV detector. The products were well separated using a reversed-phase C18 column (250 × 4.6 mm), where the mobile phase was made of acetonitrile, methanol, and water in a volume ratio of 2 : 3 : 5. The flow rate of 1 mL min^{-1} was maintained, and the injection volume was 20 μL. The content of the compounds was detected by interpolating the calibration curves.

2.5 Regeneration of the catalysts

After the completion of the reaction, the heterogeneous solid catalysts **3** and **4** were separated from the reaction mixture by filtration, washed with an excess amount of acetone (for styrene)/ethyl acetate (for phenol) and dried *in vacuo*. The recovered solid catalyst was then added to a fresh reaction mixture of phenol (5 mmol)/styrene (2 mmol) and 30% H_2O_2 (4 equivalents) to repeat the experiment under the optimized reaction conditions. The progress of the reaction was monitored by HPLC. As complexes **1** and **2** were homogeneous in the reaction mixture, there was difficulty in catalyst separation and recycling for oxidation reactions.

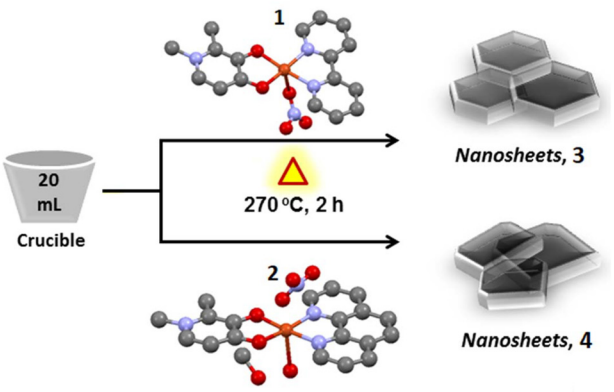

Scheme 2 Preparation of CuO NPs **3** and **4** from complexes **1** and **2**.

3. Results and discussion

3.1 Synthesis of Cu(II) complexes [Cu(def)(bpy)(NO_3)] (1) and [Cu(def)(phen)(H_2O)]NO_3·(CH_3OH) (2), and CuO nanomaterials

As illustrated in Scheme 1, the compounds **1** and **2** were synthesized following a fairly simple and direct synthetic route under reflux conditions. The reaction afforded green colored crystals appropriate for single crystal XRD analysis upon slow evaporation of the solvent from the reaction mixture. The complexes **1** and **2** were observed to be highly soluble in water and insoluble in organic solvents. After achieving the synthesis of complexes **1** and **2**, they were characterized by various spectroscopic and analytical methods such as AAS, UV-Vis, FT-IR,

EPR, HR-MS, CV, and single crystal XRD analyses as discussed below.

The synthesis of CuO nanoparticles has been achieved by the thermal degradation of complexes **1** and **2**. As shown in Scheme 2, the complexes could be transformed into the corresponding NP simply by heating at 270 °C for 2 h. The obtained product was then characterized using different physicochemical and spectral analyses. The nanomaterials **3** and **4** are insoluble in water and in common organic solvents.

3.2 Characterization of complexes 1 and 2

3.2.1 FT-IR, UV-Vis, and HRMS spectrometry. The FT-IR spectra of **1** and **2** display peaks characteristic of different stretching vibrations in the complexes. The peaks that appear in the ranges of 505–511 cm^{-1} and 535–536 cm^{-1} for both the complexes are characteristic of ν(Cu–O) and ν(Cu–N) vibrations (Fig. S1).[45,46] The peaks present in the range of 1000–1400 cm^{-1} in **1** are characteristic of the monodentatively coordinated nitrate. The weak peak appearing around 1600 cm^{-1} in **1** and the medium intensity peak around 1640 cm^{-1} are characteristic of ν(C=N) and ν(C=O) vibrations of coordinated diimine and def, respectively. The presence of a comparatively sharp band in the range of 3300–3440 cm^{-1} indicates the presence of coordinated water molecules in the complex **2**.[45,46] The UV-Vis spectra of the complexes **1** and **2** clearly show a broad band characteristic of ligand field (LF) transition in the range 630–635 nm with a very low molar absorptivity of 50 and 33 M^{-1} cm^{-1}, respectively (Fig. S2).[45] The very intense bands observed in the range 200 to 309 nm are ascribed to the intra-ligand $\pi \rightarrow \pi^*$ and $n \rightarrow \pi^*$ and LMCT transitions, as mentioned in Table 1.[47] The HR-MS data of **1** and **2** display primarily a single mass peak apparently due to the mononuclear fragment of $[Cu(def)(diimine)]^{2+}$ species, supporting the stoichiometry of the complexes and revealing that the complexes retain their mixed ligand identity even in solution (Fig. S3). The molar conductivity of **1** measured in methanol solution (Λ_M/Ω^{-1} cm^2 mol^{-1}, **1**, 140; **2**, 138) falls in the range for 1 : 1 electrolytes, supporting the displacement of coordinated nitrate of **1** in solution.[48]

3.2.2 X-ray crystal structures of 1 and 2

*Structure of [Cu(def)(bpy)(NO$_3$)] (**1**).* The crystallographic unit cell of the neutral copper(II) complex **1** contains no lattice water molecule. The ORTEP representation and numbering scheme for **1** are shown in Fig. 1 and the crystal refinement data and the selected bond lengths and bond angles are listed in Table 2 and Table S1. For complex **1**, the value of the structural index τ of 0.04 [$\tau = (\beta - \alpha)/60$, where α = O(2)–Cu(1)–N(1) = 172.5(1)° and β = O(1)–Cu(1)–N(2) = 175.1(1)°] reveals that the coordination geometry around copper(II) is a square-based

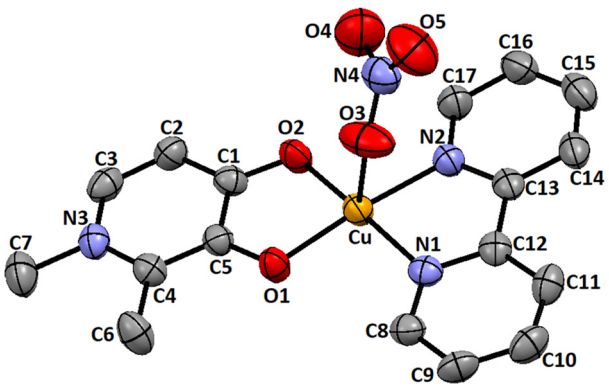

Fig. 1 ORTEP representation of the crystal structure of [Cu(def)(bpy)(NO$_3$)] **1**. Ellipsoids are drawn at 50% probability. Hydrogen atoms are omitted for clarity.

Table 1 Electronic and EPR spectral data (λ_{max} in nm, ε in M^{-1} cm^{-1}) for [Cu(def)(bpy)(NO$_3$)] (**1**) and [Cu(def)(phen)(H$_2$O)]NO$_3$·(CH$_3$OH) (**2**) in CH$_3$OH solution[a]

Complexes	λ_{max} in nm (M^{-1} cm^{-1})	Assignment	EPR[e]
[Cu(def)(bpy)(NO$_3$)] **1**	633 (50)	LF[b]	$g_{\|}$, 2.317
	202 (60 470)	Ligand-based[c]	$g_{\perp}$, 2.076
	226 (43 930)	Ligand-based[c]	$A_{\|}$, 160 × 10^{-4} cm^{-1}
	300 (24 530)	LMCT[d]	
	309 (24 070)	LMCT[d]	
[Cu(def)(phen)(H$_2$O)]NO$_3$·(CH$_3$OH) **2**	635 (30)	LF[b]	$g_{\|}$, 2.321
	202 (53 930)	Ligand-based[c]	$g_{\perp}$, 2.075
	227 (50 000)	Ligand-based[c]	$A_{\|}$ = 170 × 10^{-4} cm^{-1}
	271 (33 730)	Ligand-based[c]	
	293 (16 070)	LMCT[d]	

[a] Concentration, 0.015 mM–5 mM. [b] LF, ligand field. [c] Ligand-based dπ–π* and n–π* transitions. [d] LMCT, ligand to metal charge transfer. [e] In frozen methanol solution, at liquid nitrogen temperature; microwave frequency: 9.09 GHz.

Table 2 Crystal data and structure refinement details for [Cu(def)(bpy)(NO$_3$)] (**1**) and [Cu(def)(phen)(H$_2$O)]NO$_3$·(CH$_3$OH) (**2**)

	1	**2**
Sum formula	$C_{17}H_{16}CuN_4O_5$	$C_{20}H_{22}CuN_4O_7$
Formula weight	419.89	493.97
Temperature (K)	296(2)	296(2)
Wavelength (Å)	0.71073	0.71073
Crystal system	Monoclinic	Triclinic
Space group	$P2_1/c$	$P\bar{1}$
a (Å)	7.9387(7)	7.159(9)
b (Å)	14.0075(12)	11.629(16)
c (Å)	15.4600(13)	13.894(18)
α (°)	90	101.903(16)
β (°)	92.032(6)	101.486(17)
γ (°)	90	105.743(16)
Volume (Å^3)	1718.1(3)	1049(2)
Z	4	2
D_c (mg cm^{-3})	1.623	1.564
Reflections collected	29 410	25 017
Goodness-of-fit on F^2	1.360	1.040
Final R indices [$I > 2\sigma(I)$]	0.0522, wR_2 = 0.0952	0.0541, wR_2 = 0.1346
R indices (all data)	0.0977, wR_2 = 0.1071	0.0833, wR_2 = 0.1556
CCDC	1880241	1884417

pyramid with the corners of the CuN_2O_2 (square plane) occupied by N1 and N2 nitrogen atoms (Cu–N1, 1.973(4); Cu–N2, 1.977(4) Å) of bpy and O1 and O2 oxygen atoms (Cu–O1, 1.914(3); Cu–O2, 1.935(3) Å) of the deferiprone ligand, since for a perfect square pyramidal geometry the value of τ is zero, whereas for a perfect trigonal bipyramidal coordination geometry the τ value is unity.[49,50] The apical position is occupied by the O3 oxygen atom of the monodentatively coordinated nitrate at a longer Cu–O3 bond length of 2.490(4) Å than the equatorial oxygen atoms due to tetragonal distortion caused by the two electrons in the d_{z^2} orbital (Jahn–Teller distortion) of Cu(II). The Cu–N_{bpy} bond lengths observed in **1** [Cu–N1, 1.973(4) Å; Cu–N2, 1.977(4) Å] fall in the range of Cu–N_{imine} distances detected in the diimine complexes reported previously.[45,51,52] Also, the Cu–O_{keto} bond length 1.935(3) Å is longer than the Cu–$O_{enolate}$ bond length of 1.914(3) Å in **1**, on account of the weaker interaction of the C=O bond of deferiprone (C1=O2, 1.298(6) Å) than that of the enolate C–O bond (C5–O1, 1.337(5) Å) with Cu(II), as expected. A similar observation has been made for the [Cu(maltolate)(bpy)]$^+$ complex in which the Cu–O_{keto} bond length (1.991(15) Å) is longer than the Cu–$O_{enolate}$ bond length (1.936(11) Å).[45] Also, in the complex [Cu(sal)(bpy)]$^+$, the Cu–$O1_{carbonyl}$ bond length (1.908(3) Å) is shorter than the Cu–$O2_{phenolate}$ bond length (1.960(4) Å).[52]

Structure of [Cu(def)(phen)(H_2O)]NO_3·CH_3OH (2). The X-ray structure of **2** contains a lattice nitrate and no water molecule. The ORTEP representation and numbering scheme for **2** are shown in Fig. 2 and the crystal refinement data and the selected bond lengths and bond angles are listed in Table 2 and Table S1. There is a slight disorientation in the lattice nitrate in the crystal structure that might have originated from the multiple possible orientations with similar energies. This could have led to the co-existence of different NO_3^- anion orientations in different unit cells of the crystal. Moreover, the packing arrangement of the complex ion in the crystal lattice might have favored the multiple orientations. However, no serious alerts (alert A or B) found in checkCIF for the NO_3^- anion suggested that the disorder is properly modeled and refined during the crystallographic analysis. The Cu(II) coordination geometry is five-coordinated constituted by N1 and N2 nitrogen atoms of phen, O1 and O2 oxygen atoms of the def ligand, and the oxygen atom of the water molecule. The value of the structural index τ of 0.04 [$\tau = (\beta - \alpha)/60$, where α = O(2)–Cu(1)–N(1) = 172.3(1)° and β = O(1)–Cu(1)–N(2) = 175.0(1)°] reveals that the coordination geometry around Cu(II) is also a square-based pyramid, as for its bpy analog **1** where the corners of the CuN_2O_2 square plane is occupied by the N1 and N2 nitrogen atoms of phen and the O1 and O2 oxygen atoms of deferiprone.[45,50] The Cu–N (1.989(4), 2.011(4) Å) and Cu–O (1.903(4), 1.948(4) Å) bond lengths and bond angles are similar to those of its analogous bpy complex **1** while the Cu–OH_2 bond length (2.439(5) Å) is longer than the equatorial Cu–N and Cu–O bond lengths, which is typical of the occupation of two electrons in the d_{z^2} orbital (Jahn–Teller distortion) of Cu(II). The mean bond length of Cu–N_{phen} = 2.0 Å and the bite angle N1–Cu–N2 = 82.65(15)° are in accordance with those of the previously reported [Cu(acac)(phen)NO_3] complex (82.0(13)°)[53] and [Cu(phen)(maltol)]$^+$ complex (83.3(3)°).[45] The shortest C–C bond present in the molecule is the C(12)–C(13) bond (1.355(8) Å), whereas the adjacent C(12)–C(11) and C(13)–C(14) bonds of 1.416(7) and 1.431(7) Å are considerably longer. Thus, the phen molecule in complex **2** can be considered as a bpy molecule fused by a C–C bond with a predominant double bond character.[53] Similar to **1**, the Cu–O_{keto} bond (1.948(4) Å) is longer than the Cu–$O_{enolate}$ bond (1.903(4) Å) in **2**, on account of the stronger interaction of the enolate group with Cu(II) than the C=O group of deferiprone (C1=O2, 1.310(5); C5–O1, 1.323(5) Å). A similar observation has been made also for [Cu(maltolate)(phen)]$^+$ with the Cu–O_{keto} bond length (1.985(6) Å) being longer than the Cu–$O_{enolate}$ bond length (1.961(7)) Å.[45]

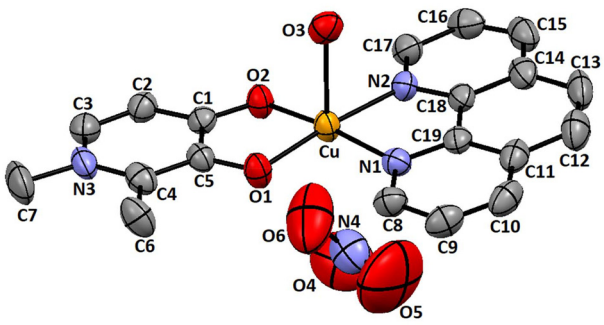

Fig. 2 ORTEP representation of the crystal structure of [Cu(def)(phen)(H_2O)]NO_3·(CH_3OH) **2**. Ellipsoids are drawn at 50% probability. Methanol and hydrogen atoms are omitted for clarity.

3.2.3 EPR spectroscopy. The frozen EPR spectra of complexes **1** and **2** (Fig. S4 and Table 1) were recorded in frozen CH_3OH : acetone solution (4 : 1 v/v) at LNT. In general, for Cu(II) complexes with a square-based CuN_4 chromophore, the $g_\parallel$ and $A_\parallel$ values are expected to be observed at 2.200 and 180–200 × 10^{-4} cm^{-1}, and the replacement of the two nitrogen atoms in this chromophore by two oxygen atoms to give a CuN_2O_2 chromophore is expected to lower the $g_\parallel$ and decrease the $A_\parallel$ values.[45,48] Thus, for the complexes [Cu(sal)(diimine)]$^+$ (Hsal = salicylaldehyde; diimine = bpy, phen) with a CuN_2O_2 chromophore, lower $g_\parallel$ and higher $A_\parallel$ values (bpy: $g_\parallel$, 2.228; $A_\parallel$, 181 × 10^{-4} cm^{-1}; phen: $g_\parallel$, 2.235; $A_\parallel$, 182 × 10^{-4} cm^{-1}) have been observed, with no significant distortion from planarity ($g_\parallel/A_\parallel$ = 117–124 cm).[52] However, the higher $g_\parallel$ (**1**, 2.317; **2**, 2.321) and lower $A_\parallel$ values observed (**1**, 160; **2**, 170 × 10^{-4} cm^{-1}) for **1** and **2**, which are consistent with the square planar geometry (*cf.* above), and the π-back bonding of Cu(II) with the conjugated carbonyl group of def result in enhanced π-delocalization of electron density from bpy and phen through the Cu(II) nucleus to def, and hence the decreased interaction between Cu(II) and the unpaired electron.[54] The value of G [= $(g_\parallel - 2)/(g_\perp - 2)$ = 4.17 (**1**), 4.28 (**2**)] supports the presence of a square-based geometry around Cu(II), which is evident from the X-ray crystal structures of the complexes. So, the higher value of the $g_\parallel/A_\parallel$ quotient observed (**1**, 137; **2**,

145 cm) should correspond to the enhanced π-back bonding of Cu(II) in the square-based CuN_2O_2 chromophore with no striking distortion from planarity, as observed from the X-ray crystal structures of **1** and **2**. Similar observations have been made for the complexes $[Cu(maltol)(diimine)]^+$ (diimine = bpy, phen)[45] with a CuN_2O_2 chromophore formed by maltolate with a conjugated π-carbonyl group similar to that in the flavonolate moiety (bpy: $g_{\|}$, 2.300; phen: $g_{\|}$, 2.310). Higher $g_{\|}$ and lower $A_{\|}$ values were observed for the complexes $[Cu(tdp)(diimine)]^+$ (H(tdp)) = 2-[(2-(2-hydroxyethylamino)-ethylimino)methyl] phenol; diimine = bpy, phen) with a square-based CuN_2O_2 chromophore (bpy: $g_{\|}$, 2.230; $A_{\|}$, 185 × 10^{-4} cm^{-1}; phen, $g_{\|}$, 2.237; $A_{\|}$, 174 × 10^{-4} cm^{-1}) and more planar geometry ($g_{\|}/A_{\|}$, 121–129 cm).[51]

3.2.4 Electrochemical studies. The cyclic voltammetry (CV) studies of complexes **1** and **2** were performed using a three-electrode system comprising a glassy carbon electrode as the working electrode, Pt-wire as the counter electrode, Ag/AgCl as the reference electrode, and using 0.1 M TBAB (tetra-butylammonium bromide) as a supporting electrolyte (Fig. S5 and Tables S2, S3). On scanning the potential from −0.4 to 0.4 V *vs*. Ag/AgCl, the CV for **1** and **2** displays a quasi-reversible (ΔE_p, **1**: 85; **2**: 77 mV) redox wave characteristic of a Cu(II)/Cu(I) redox couple.[45] The higher π-delocalized phen ring in **2** is expected to stabilize Cu(I) more than the non-planar and more strongly σ-bonding pyridyl rings in **1** (*cf.* below), rendering its Cu(II)/Cu(I) redox potential more positive. However, the $E_{1/2}$ value of **1** (0.075 V) is higher than that of **2** (−0.118 V), revealing that the reduction of Cu(II) in the former complex is more facile than that of Cu(II) in the latter.

So, it is evident that the reduction of Cu(II) in the complexes takes place after the dissociation of the axially bound water molecule in solution.[54] The dissociation of the axial water molecule, which is more weakly bound in **1** (Cu-ONO_2, 2.490 Å, coordinated nitrate displaced by water in solution) than in **2** (Cu–O3(H_2O), 2.439 Å, *cf.* above) requires lower energy, as observed from the X-ray crystal structure, rendering the Cu(II)/Cu(I) redox potential of **1** more positive.

3.3 Characterization of CuO NPs 3 and 4

3.3.1 Powder X-ray diffraction studies. The obtained nanomaterials were characterized by XRD analysis and the diffractograms are shown in Fig. 3. The XRD pattern of **3**, as shown in Fig. 3(a), displayed diffraction peaks located at 2θ values of 32.4, 35.4, 38.6, 48.7, 53.4, 58.1, 61.4, 65.9, and 67.9 attributable to (110), (002), (111), (202), (020), (202), (113), (311), and (220) planes, which are characteristic of a monoclinic phase (JCPDS = 895895 and 45-0937) as shown in Fig. S6.[55–58] The XRD patterns revealed a high crystallinity of the material[59] and also indicated the purity of the CuO nanocrystals generated,[60,61] as no impurity peaks were detected in the diffractogram. Similar results were reported previously by Park and co-workers during the preparation of CuO nanocatalysts.[62] The XRD pattern of **4** exhibited a close analogy with that of **3** as illustrated in Fig. 3(b). Thus, the XRD patterns of both synthesized materials testified the formation of pure CuO nanomaterials.

3.3.2 FT-IR spectroscopy. In the FT-IR spectra of **3** and **4**, the appearance of peaks between 1626 and 1633 cm^{-1} characteristic of the stretching vibrations of the Cu–O bonds of Cu(II) oxide NPs (Fig. S7) and the presence of a strong absorption band in the range of 530 to 534 cm^{-1} and at 1017 cm^{-1} corresponding to different Cu–O bending vibrations indicated the formation of the targeted NPs.[63,64] Similar observations were made previously by Raul *et al.* in the case of the synthesis of CuO nanorods.[64]

3.3.3 Diffuse reflectance UV-visible analysis. The diffuse reflectance UV-visible spectra of both the materials **3** and **4** showed a characteristic d–d transition absorption band at a higher wavelength (700–800 nm) due to the Cu(II) species ($3d^9$) (Fig. S8).[62,65] In addition, lower wavelength absorption bands were also observed in the range of 245–260 nm corresponding to the charge transfer from $O^{2-} \rightarrow Cu^{2+}$ in both the nanocatalysts.[66]

3.3.4 Scanning electron microscopy (SEM) and transmission electron microscopy (TEM) analyses. The SEM ana-

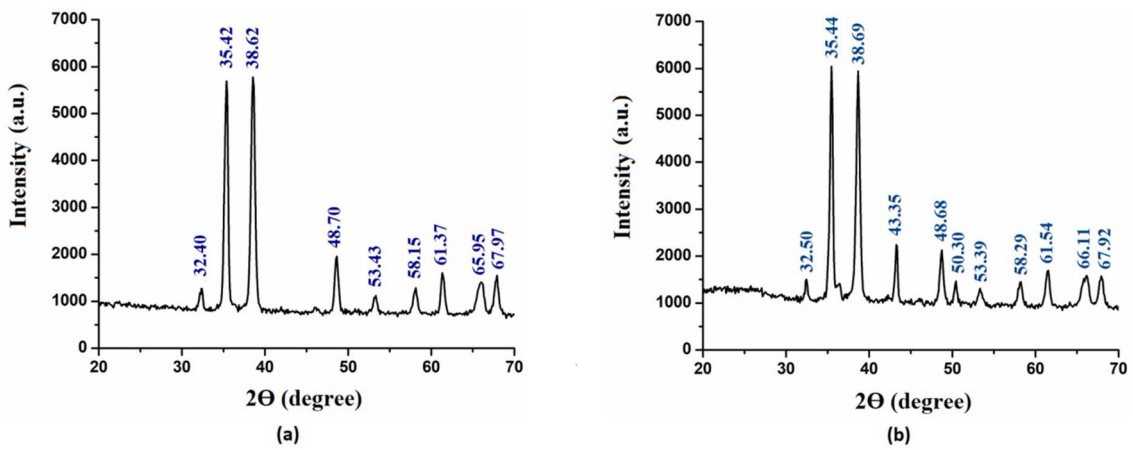

Fig. 3 Powder XRD patterns of CuO NPs **3** (a) and **4** (b).

lyses were employed to determine the surface morphology of the synthesized nanomaterials. The SEM images of **3** and **4** shown in Fig. 4(a) and 5(a) exhibit a typical nanosheet-like structure as has been reported previously.[60]

Further information regarding the morphology and nano-dimensions of the synthesized nanomaterials was derived by carrying out TEM measurements. The nano-sheet-like morphology of the synthesized nanomaterials was further evident from the TEM images of the materials presented in Fig. 4(b, c) and 5(b, c). The high-resolution TEM image of **4** shows that the phase distance between the adjacent lattice fringes has a value of 0.25 nm (Fig. 5(c)). The appearance of dark regions in the TEM images of both materials is a consequence of stacking among a few nanosheets, as has been observed previously by Sedaghati and co-workers during the synthesis of CuO nanosheets.[67] These results are in good agreement with the lattice *d*-spacing measurement from the HRTEM analysis reported earlier by Qian *et al.*[60] and Zhang *et al.*[68] These findings were further supported by the results of our XRD analysis shown in Fig. 3(b).

3.3.5 BET analysis. In order to determine the surface area of the two nanomaterials, N_2-adsorption–desorption isotherms were recorded (Fig. 6 and 7). Both the synthesized nanomaterials were found to exhibit a typical type II isotherm pattern.[69] The BET surface area analysis of the two synthesized nanosheets provided a surface area of 20.8 $m^2\ g^{-1}$ for **3** and 12.5 $m^2\ g^{-1}$ for **4**, respectively. The obtained surface area values were found to be in accord with the reported results for CuO nanomaterials.[58,70] In general, the commercial CuO powder displays a surface area of ~0.1 $m^2\ g^{-1}$;[71] however, the CuO synthesized by our protocol leads to a multifold enhancement in the surface area which is desirable from the catalysis point of view. The overall pore size distribution (PSD) of **3** and **4** was also determined by using the BJH model. The PSD for **3** was found to be in the range of 1.6–7.0 nm, whereas **4** exhibited a PSD between 1.6 and 5.3 nm (ref. 72) as witnessed from the respective BJH plots in Fig. 6(b) and 7(b). The pore diameter values obtained from the BJH method also indicated the presence of slight mesoporosity in both the nanomaterials.

3.4 Catalytic activity of the precursor complexes 1 and 2, and nanomaterials 3 and 4 in organic oxidations

3.4.1 Styrene epoxidation. The activity of the soluble mixed ligand Cu complexes **1** and **2** as well as their transformed products, CuO nanocatalysts **3** and **4**, in styrene epoxidation, was investigated with or without solvent under a variety of reaction conditions. For optimization of the reaction conditions for maximum styrene conversion, the complex **2** was used as a representative catalyst, and the effects of reaction parameters

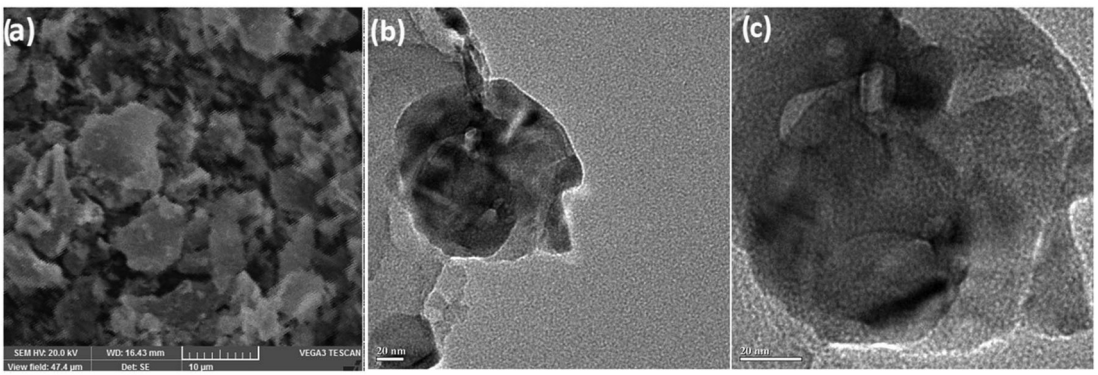

Fig. 4 SEM (a) and TEM (b and c) images of CuO NP **3**.

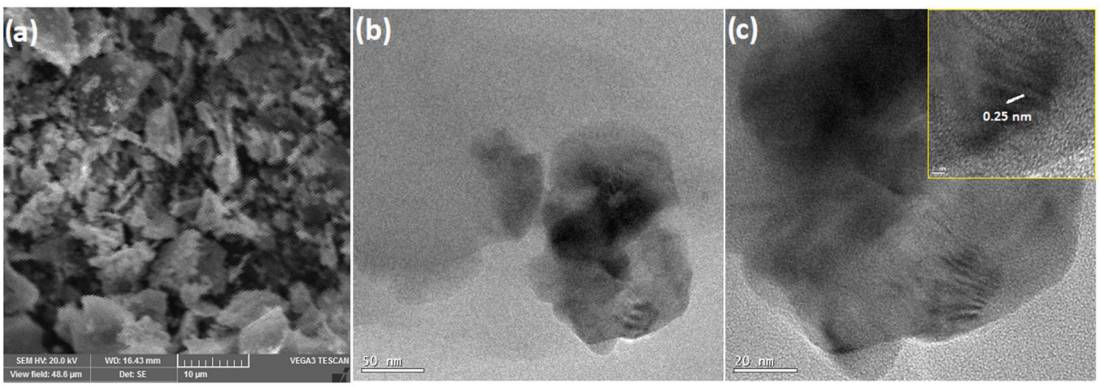

Fig. 5 SEM (a) and TEM (b and c) image of CuO NP **4**.

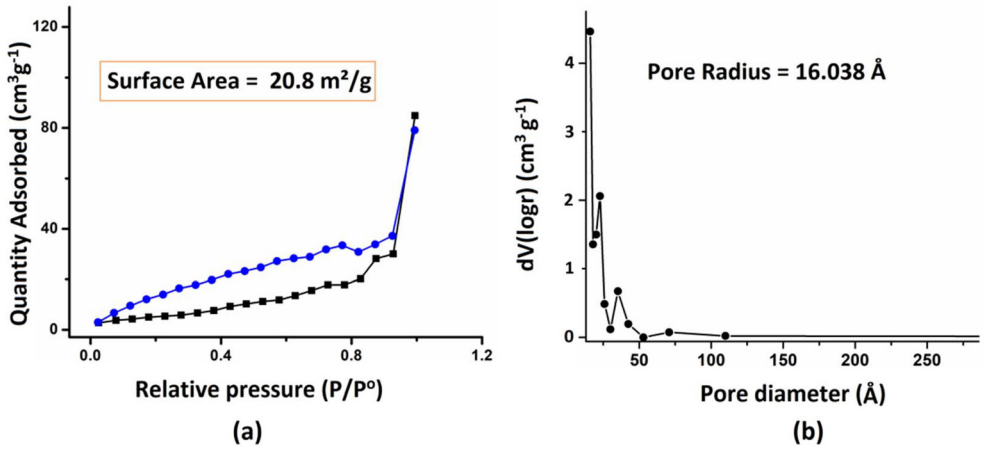

Fig. 6 BET (a) and BJH (b) plots of CuO NP **3**.

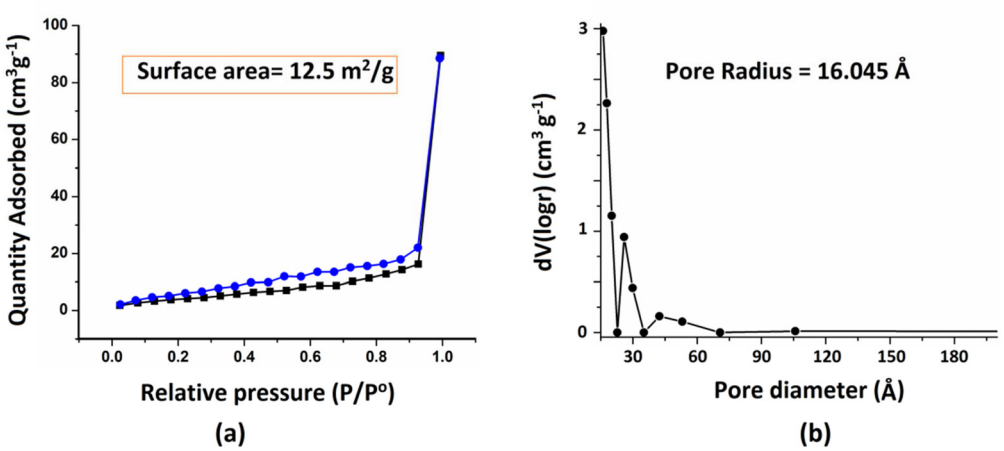

Fig. 7 BET (a) and BJH (b) plots of CuO NP **4**.

such as time, concentration of oxidant, reaction temperature, catalyst amount, and solvent nature were evaluated.

Effect of solvent. To study the solvent effect, apart from conducting the reaction under solvent-free conditions, we have used the universal green solvent water and a set of relatively safer organic solvents. The synthesized nanomaterials **3** and **4** were observed to be insoluble in water and in common organic solvents. On the other hand, the water-soluble precursor complexes **1** and **2**, although insoluble in neat organic solvents, dissolved completely in water-miscible organic solvents, such as methanol, ethanol, and acetonitrile, in the presence of aqueous H_2O_2. For comparison, the initial reactions were performed under identical conditions keeping a catalyst : substrate molar ratio of 1 : 1000 and a substrate : oxidant molar ratio of 1 : 4 at 60 °C. As seen from the results presented in Fig. 8 and Table S4 (entries 1–4) the catalyst displayed remarkable efficiency and compatibility in organic and aqueous media providing high styrene conversion along with excellent epoxide selectivity, in each of the solvents tested. Since the epoxide selectivity % is above 97% (Table S4, entries 1, 3, and 4) with complex **2**, it is expected that only a few or no ring opening products would be formed in the presence of H_2O or the alcoholic solvents.

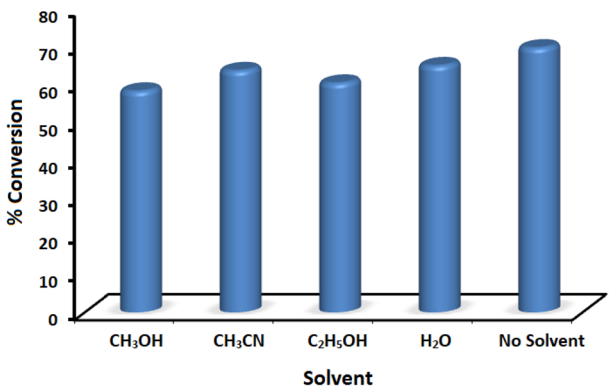

Fig. 8 Effect of solvent on styrene epoxidation. Reaction conditions: styrene (2 mmol), catalyst **2** (0.002 mmol), H_2O_2 (8 mmol), 60 °C, solvent (3 mL), and 6 h.

Nevertheless, it was gratifying to note that the best results in terms of conversion as well as nearly 99% epoxide selectivity were achieved under solventless conditions (Table S4, entry 5) along with reasonably high TON and TOF values (697 and 116.2 h^{-1}). Relatively higher efficiency of a solvent-free procedure is not unusual,[73] which may be linked to the restricted motion of the reactants in the absence of solvent inside the reaction mixture. Consequently, based on these findings, we proceeded to investigate the activity of the catalyst in subsequent reactions under solvent-free conditions.

Effect of reaction temperature. The effect of reaction temperature on the styrene conversion was assessed at four different reaction temperatures initiating from room temperature as shown in Fig. 9 and Table S4 (entries 5–8) keeping other parameters fixed. While no conversion was noted at room temperature, an increase in temperature resulted in a gradual rise in % conversion. More than 97% conversion with nearly 100% selectivity could finally be obtained with TON and TOF values as high as 973 and 162.2 h^{-1}, respectively at 80 °C. Thus, the reaction temperature of 80 °C was considered to be optimal for the catalytic epoxidation process.

Effect of reaction time. The trend observed after monitoring the % conversion of styrene as a function of time over a span of 6 h is illustrated in Fig. 10, and also in Table S4 (entries 8–13). Initially, as seen from the data (Table S4, entry 9), the reaction proceeded rapidly leading to 69.3% conversion within 1 h of starting the reaction with 98.7% epoxide selectivity. The resulting high TOF value of 693 h^{-1} obtained within the initial 1 h of the reaction is indeed noteworthy. On extending the reaction time, the conversion increased steadily until >97% conversion was attained after 6 h, with nearly 100% styrene oxide selectivity. These findings demonstrated the high stability of the catalyst, as reflected by its ability to retain its high activity and selectivity even after extending the reaction up to 6 h at a fairly elevated temperature of 80 °C.

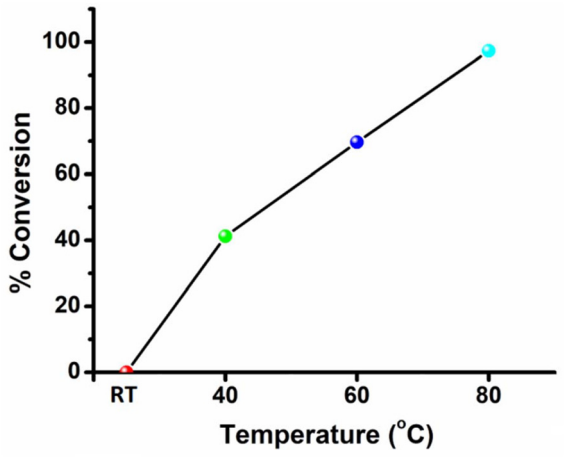

Fig. 9 Effect of the temperature on styrene epoxidation. Reaction conditions: styrene (2 mmol), catalyst **2** (0.002 mmol), H_2O_2 (8 mmol), and 6 h.

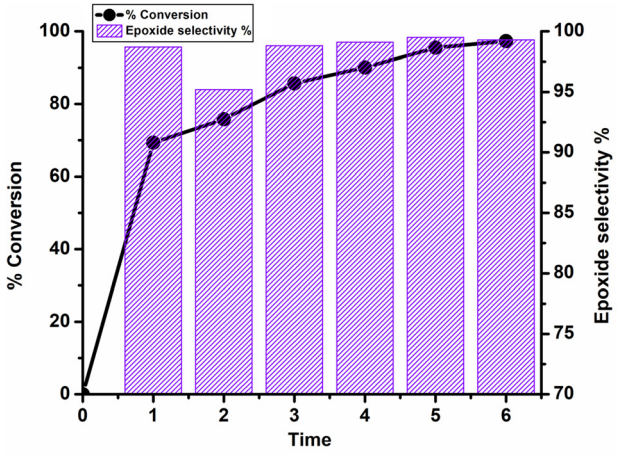

Fig. 10 Effect of reaction time on styrene epoxidation. Reaction conditions: styrene (2 mmol), catalyst **2** (0.002 mmol), H_2O_2 (8 mmol), and 80 °C.

Effect of H_2O_2 concentration. A steady rise in % conversion was observed on increasing the H_2O_2 concentration from 1 to 5 equivalents with respect to styrene in the absence of solvent, as shown in Fig. 11 and Table S4 (entries 8 and 14–17). At 4 equivalents of H_2O_2, the % conversion reached up to 97.3% with a % styrene oxide selectivity of 99.3%. Although the highest conversion reached up to 99.9% with 5 equivalents of H_2O_2, the resulting TON and TOF values (Table S4, entry 17) were not significantly higher than the values obtained using 4 equivalents of H_2O_2. Therefore, considering these facts and the environmental aspect, we decided to maintain an oxidant : substrate molar ratio of 1 : 4 for the rest of the epoxidation reactions.

Effect of catalyst amount. Next, the reaction was scrutinized under different catalyst concentrations by keeping other variables constant and the results are depicted in Fig. 12 and Table S4 (entries 8 and 18–20). It is apparent from the data that, even with a catalyst : substrate ratio as low as 1 : 2000

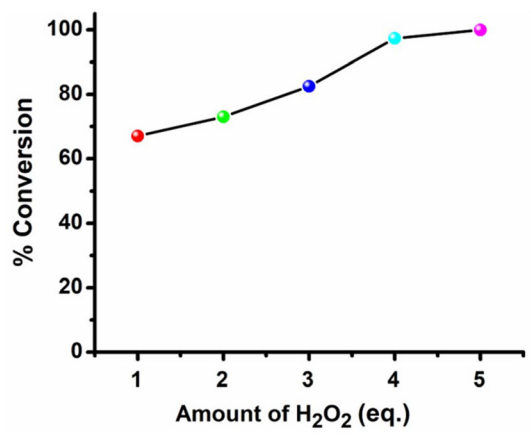

Fig. 11 Effect of H_2O_2 concentration on styrene epoxidation. Reaction conditions: styrene (2 mmol), catalyst **2** (0.002 mmol), 80 °C, and 6 h.

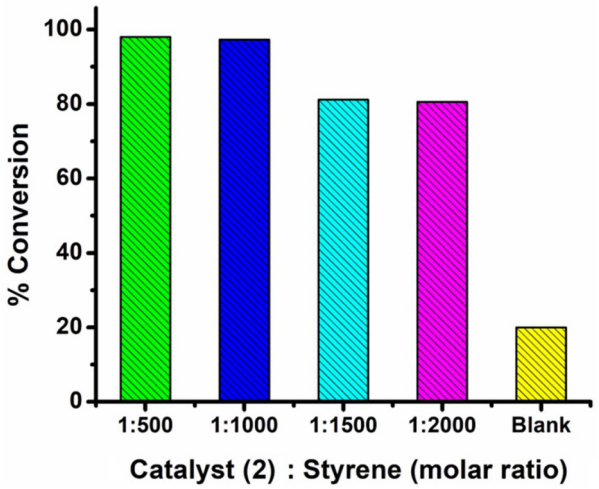

Fig. 12 Effect of the amount of catalyst **2** on styrene epoxidation. Reaction conditions: styrene (2 mmol), H_2O_2 (8 mmol), 80 °C, and 6 h.

(0.001 mmol of catalyst), a high styrene conversion of 80.6% with >98% epoxide selectivity could be achieved. On further increase in the catalyst amount to a catalyst : styrene ratio of 1 : 1000, a significant leap in styrene conversion (>97%) resulting in a high TON of 973 and a TOF of 162.2 h^{-1} was observed. However, only a marginal improvement in conversion was noted on the further increment of the catalyst amount up to a molar ratio of 1 : 500, which was also accompanied by a drastic fall in the TOF value to 81.7 h^{-1}. Therefore, a catalyst : styrene ratio of 1 : 1000 was chosen as optimal for further epoxidation reaction. The result obtained for a blank reaction performed under non-catalyst conditions confirmed the importance of the catalytic system in facilitating the reaction, as just 20% conversion of styrene occurred within the specified reaction time under standardized conditions.

*Activity of nanocatalysts **3** and **4** and complex **1** in styrene oxidation under optimized conditions.* Having standardized the reaction conditions for styrene epoxidation with the homogeneous catalyst **2**, we have sequentially performed the epoxidation reaction using the solid CuO nanocatalysts **3** and **4**, in addition to the catalyst **1**, under solvent-free conditions. In the case of the oxidation reactions with nanocatalysts **3** and **4**, 1 mg of catalyst was found to be optimal in each case, keeping all other variables constant. The excellent activity of the nanocatalysts is evident from the data presented in Table 3 (entries 3 and 4) as nearly total conversion of styrene (99.7%) could be accomplished with 99.3% epoxide selectivity with each of the catalysts. Thus, all four newly developed Cu catalysts, irrespective of being homogeneous or heterogeneous, proved to be highly effective in styrene oxidation with 30% H_2O_2 under reasonably mild reaction conditions, in the absence of organic solvent.

3.4.2 Hydroxylation of phenol. Encouraged by the excellent catalytic activity exhibited by the homogeneous catalysts **1** and **2** as well as the heterogeneous nanocatalysts **3** and **4** in styrene epoxidation, we considered it imperative to explore the versatility of the developed catalysts by examining their efficacy in the hydroxylation of phenol.

Table 3 Selective oxidation of styrene to styrene epoxide with 30% H_2O_2, catalyzed by homogeneous catalysts **1** and **2**, and heterogeneous nanocatalysts **3** and **4** [a]

Entry	Catalyst[b]	% Conversion	Epoxide selectivity%	TON[c]	TOF[d] (h^{-1})
1	**1**	98.5	99.0	985.0	164.2
2	**2**	97.3	99.3	973.0	162.2
3	**3**	99.7	99.3	—	—
4	**4**	99.7	99.3	—	—

[a] Reactions were carried out with 2 mmol of the substrate under solvent-free conditions with H_2O_2 (8 mmol). [b] Catalyst amount: 0.002 mmol (**1** and **2**), 1 mg (**3** and **4**), 6 h and 80 °C. [c] TON (turnover number) = millimoles of the product per millimole of the catalyst. [d] TOF (turnover frequency) = millimoles of the product per millimole of the catalyst per hour.

Initially, exploratory experiments were performed using each of the soluble Cu(II) complexes, **1** and **2** as well as nanocatalysts **3** and **4**, by conducting the reaction of phenol with 30% H_2O_2 in the absence of solvent, maintaining the phenol : oxidant molar ratio at 1 : 4 and catalyst : substrate ratio at 1 : 250 at 60 °C. Under these conditions, however, the reaction became highly exothermic, leading to rapid decomposition of H_2O_2 accompanied by the degradation of the reaction products. We have, therefore, examined the reaction in the presence of a variety of solvents and proceeded to optimize the other relevant reaction parameters using complex **2** as the catalyst.

Effect of solvent. The solvent effect on the catalytic performance of **2** in phenol hydroxylation was investigated by using both polar protic and nonpolar solvents such as water, methanol, acetonitrile and dichloromethane, under otherwise identical reaction conditions. The results of our assessment of solvent effects are illustrated in Fig. 13 and Table S5.

As revealed by the data, in a reaction conducted maintaining the phenol : oxidant molar ratio at 1 : 4 and catalyst : substrate ratio at 1 : 250 at 60 °C under magnetic stirring, the catalyst provided reasonably good conversion of 53.8% with the highest CT selectivity of 71.4% (Table S5, entry 1) in aqueous medium. Among the organic solvents, the maximum conversion was achieved in CH_3CN and to a lesser extent in CH_2Cl_2, whereas in CH_3OH very little product formation occurred. As has been already mentioned, the water-soluble catalyst **2**, despite its insolubility in neat organic solvents, dissolves in water miscible organic solvents in the presence of aqueous H_2O_2, providing homogeneity of the reaction solution. It is however difficult to comment on the cause or identify exactly which property of the solvent influenced the course of the reaction the most. Thus, based on our survey of the solvent effect and keeping in view the environmental compatibility of the water-based reactions, we have carried out subsequent oxidations using water as a medium of choice.

Effect of H_2O_2 concentration. A concentration dependent study with respect to the oxidant : substrate stoichiometry,

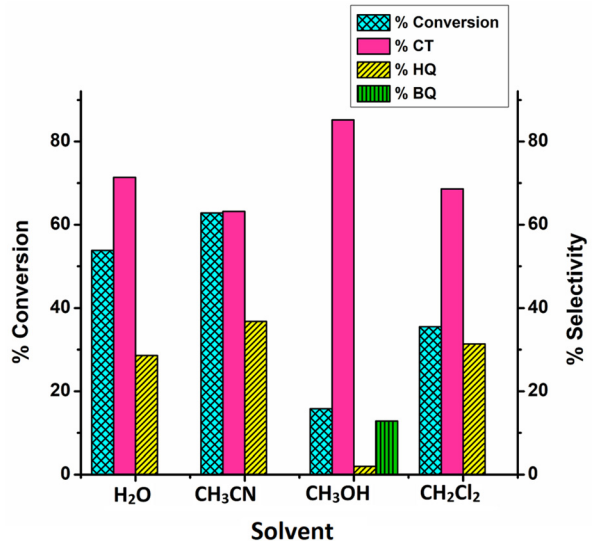

Fig. 13 Effect of solvent on phenol hydroxylation. Reaction conditions: phenol (5 mmol), catalyst **2** (0.02 mmol), H_2O_2 (20 mmol), 60 °C, solvent (3 mL), and 2 h.

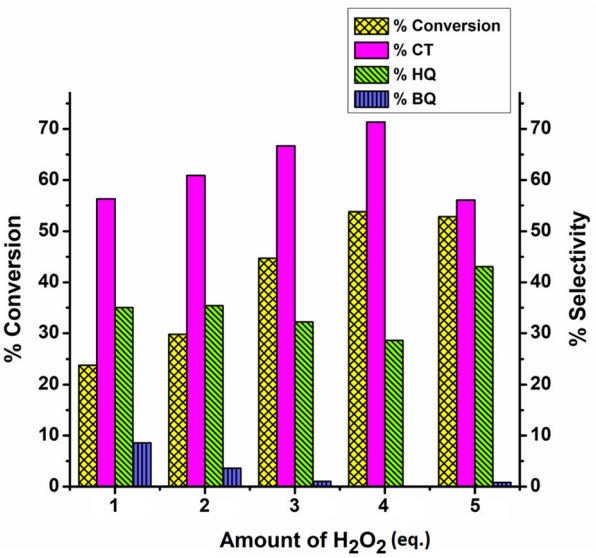

Fig. 14 Effect of H_2O_2 concentration on phenol hydroxylation. Reaction conditions: phenol (5 mmol), catalyst **2** (0.02 mmol), 60 °C, H_2O (3 mL), and 2 h.

using five different equivalents of 30% H_2O_2 under analogous reaction conditions (Fig. 14), revealed 4 equivalents of oxidant as optimal in order to obtain the highest % conversion and 100% selectivity towards the desired dihydroxybenzene (DHB) products, CT and HQ [Table S5 (entries 1 and 5–8)]. Further increase of H_2O_2 from 4 to 5 equivalents resulted in a slight decrease in the % conversion. The observation is attributable to the dilution of reacting species occurring due to the increasing volumes of H_2O_2 added to the reaction mixture, beyond the optimum requirement. Such a dilution effect is not unusual in the case of metal catalyzed H_2O_2 induced organic transformations, as shown in previous reports.[74,75]

Effect of catalyst amount. The amount of catalyst used was observed to affect the rate of phenol hydroxylation substantially (Fig. 15). As is evident from the data listed in Table S5 (entries 1 and 9–11) a 1 : 250 catalyst : substrate ratio proved to be most favorable, since on lowering the catalyst concentration to 1 : 500, there was a drastic fall in the % conversion. On the other hand, on increasing the catalyst concentration to a 1 : 100 catalyst : substrate ratio, the reaction was found to be highly exothermic. Nevertheless, it is noteworthy that a reasonably good phenol conversion with the highest TON and TOF values of 474.3 and 238.1 h^{-1}, respectively, could be attained even at a very low catalyst : phenol ratio of 1 : 1500 (Table S5, entry 9) testifying the high catalytic efficiency of the complex used. A blank reaction performed under these identical conditions demonstrated a negligible % conversion of phenol (0.45%).

Effect of reaction temperature. The % conversion and product selectivity profile of phenol as a function of temperature are shown in Fig. 16. The results revealed that while the conversion of phenol achieved at room temperature was recorded to be only 4.5% (Table S5, entry 12), on increasing the temperature to 80 °C, there was a gradual rise in % conversion of phenol up to 69.3% (Table S5, entry 14). The reaction was found to be highly exothermic above 80 °C, leading to rapid decomposition of H_2O_2. Thus, the best results with high CT selectivity and an appreciable TON of 173.5 and a TOF of 86.7 h^{-1} were obtained at 80 °C. Therefore, the moderately elevated temperature of 80 °C appeared to be optimal in phenol hydroxylation as well, which is similar to our finding in the case of styrene oxidation using the same catalyst.

Effect of reaction time. The progress of the reaction studied with respect to time over a period of 8 h is depicted in Fig. 17. As is evident from the data, the fast reaction occurring within the initial 2 h of starting the reaction provided a substantially

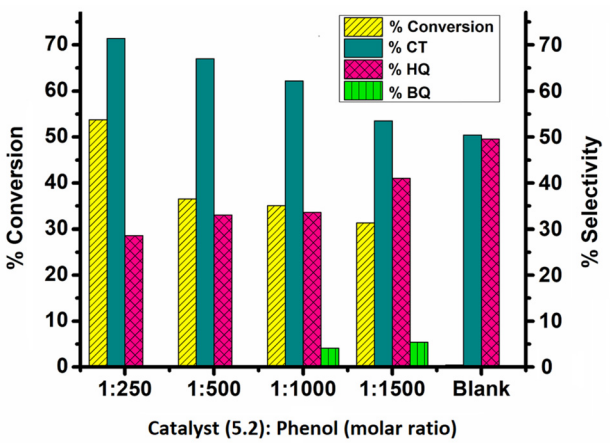

Fig. 15 Effect of the amount of catalyst **2** on phenol hydroxylation. Reaction conditions: phenol (5 mmol), H_2O_2 (20 mmol), 60 °C, H_2O (3 mL), and 2 h.

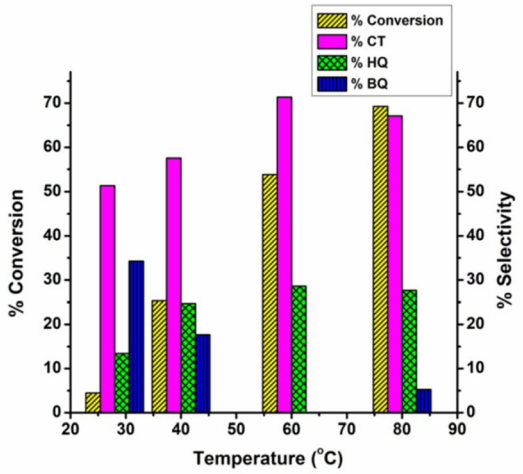

Fig. 16 Effect of the temperature on phenol hydroxylation. Reaction conditions: phenol (5 mmol), catalyst **2** (0.02 mmol), H_2O_2 (20 mmol), H_2O (3 mL), and 2 h.

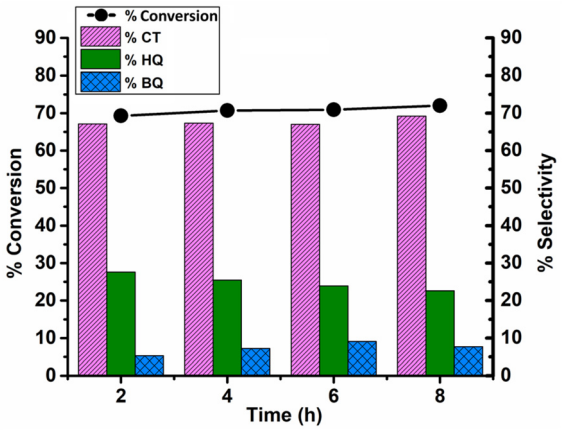

Fig. 17 Effect of reaction time on phenol hydroxylation. Reaction conditions: phenol (5 mmol), catalyst **2** (0.02 mmol), H_2O_2 (20 mmol), 80 °C, and H_2O (3 mL).

good phenol conversion of >69% with a TON of 173.5 and a DHB selectivity of >94%. Interestingly, on further extending the reaction beyond 2 h, no significant improvement in % conversion was observed and CT : HQ selectivity remained nearly constant (Table S5 and entries 14–17), whereas the TOF value decreased to 22.5 h^{-1}. Thus, these results clearly revealed 2 h of reaction time to be optimal for phenol hydroxylation under the reaction conditions maintained in aqueous medium.

*Activity of nanocatalysts **3** and **4** and complex **1** in phenol hydroxylation under optimized conditions.* Subsequent to the optimization of the right conditions for phenol hydroxylation using catalyst **2**, we further proceeded to evaluate the efficiency of the homogeneous catalyst **1** and heterogeneous nanocatalysts **3** and **4** in aqueous medium. For the CuO nanocatalysts **3** and **4**, 10 mg of catalyst was observed to be optimal under otherwise identical reaction conditions. To our satisfaction, all the four catalysts displayed comparable results with respect to % phenol conversion as seen in Table 4. Interestingly, however, the nanocatalysts displayed superior selectivity towards the desired DHB products (100% selectivity), whereas the homogeneous catalysts **1** and **2** showed 93 and 94.7% selectivity towards DHB, respectively, with benzoquinone being the minor oxidation product (Table 4).

3.4.3 Recyclability of the catalysts. For the practical utility of a catalytic procedure, the stability and recyclability of the catalyst are of paramount importance. Although the homogeneous catalysts usually display superior activity *vis-a-vis* their heterogeneous counterpart, their recovery is often difficult requiring a tedious separation process from organic products.[76,77] In the present study, notwithstanding the excellent activity displayed by the homogeneous complexes **1** and **2** in styrene epoxidation, the catalysts could not be recovered for reuse in subsequent cycles of reaction.

On the other hand, the heterogenized nanocatalysts **3** and **4** enabled easy recovery from the spent reaction mixture by simple filtration. The reusability of the catalysts was tested independently in styrene epoxidation under respective optimized reaction conditions. The recovered catalysts **3** or **4** after washing with acetone were dried under vacuum. The catalyst was then recharged in a subsequent reaction run without further conditioning. The recyclability of the heterogeneous catalysts was tested up to three reaction cycles in the case of solvent-free styrene epoxidation.

The results presented in Fig. 18 and 19 demonstrate that both the catalysts **3** and **4** retained epoxide selectivity undiminished up to the third reaction cycle. The activity of both the

Table 4 Phenol hydroxylation with 30% H_2O_2 catalyzed by homogeneous catalysts **1** and **2** and nanocatalysts **3** and **4** [a]

			% Selectivity				
Entry	Catalyst[b]	% Conversion	CT	HQ	BQ	TON[c]	TOF[d] (h^{-1})
1	**1**	63.2	67.0	26.0	7.0	157.9	78.9
2	**2**	69.3	67.1	27.6	5.2	173.5	86.7
3	**3**	65.9	71.1	28.9	0	—	—
4	**4**	67.8	76.3	23.7	0	—	—

[a] Reactions were carried out with 5 mmol of substrate in H_2O and H_2O_2 (20 mmol). [b] Catalyst amount: 0.02 mmol (**1** and **2**), 10 mg (**3** and **4**), 2 h and 80 °C. [c] TON (turnover number) = millimoles of the product per millimole of the catalyst. [d] TOF (turnover frequency) = millimoles of the product per millimole of the catalyst per hour.

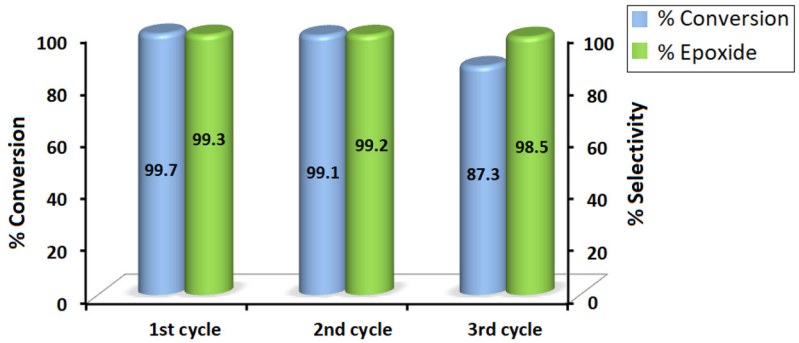

Fig. 18 Recyclability of compound **3** for the epoxidation of styrene.

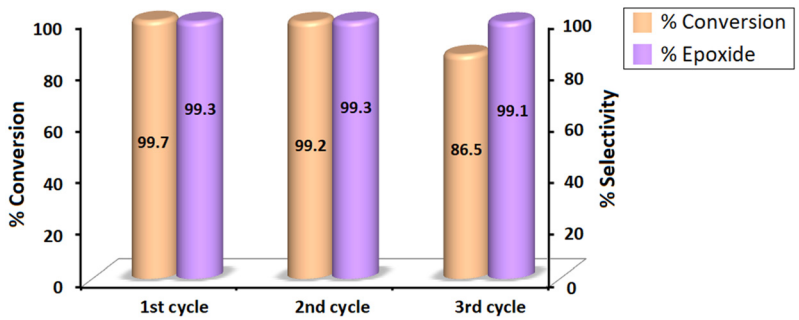

Fig. 19 Recyclability of compound **4** for the epoxidation of styrene.

catalysts on the other hand, as reflected by the % styrene conversion shown in Fig. 18 and 19, after remaining nearly unaltered in the second reaction cycle, showed a slight decrease in the subsequent cycle of reaction. Thus, considering the long reaction duration of 6 h and the elevated temperature of 80 °C at which each cycle of solvent-free epoxidation was conducted, the observed recyclability of the catalyst for at least three cycles of reaction is noteworthy.

In the case of phenol hydroxylation carried out in aqueous medium, the recycled catalysts after showing almost consistent % conversion and % DHB selectivity in the second catalytic cycle displayed a gradual decline in % conversion and an alteration in the CT : HQ selectivity ratio in subsequent cycles as shown in Fig. 20 and 21. Nevertheless, the reactions proceeded with a consistent 100% DHB selectivity with CT and HQ being the only products up to the 3rd cycle of reaction. In the 4th reaction cycle, however, the reaction product also contained a small amount of benzoquinone along with CT and HQ obtained as major products.

The regenerated catalysts were also characterized by IR spectral analysis. The FT-IR spectral data of the regenerated catalysts exhibited the characteristic peaks that were present in the pristine catalysts **3** and **4** (Fig. S9–S12), indicating that the catalysts retain their structural integrity during the catalytic process. Moreover, no further conversion was noted after the separation of the solid catalyst from the reaction mixture, allowing the reaction to continue for another 1 h under optimized conditions. These results demonstrate the heterogeneous nature of the catalytic process.

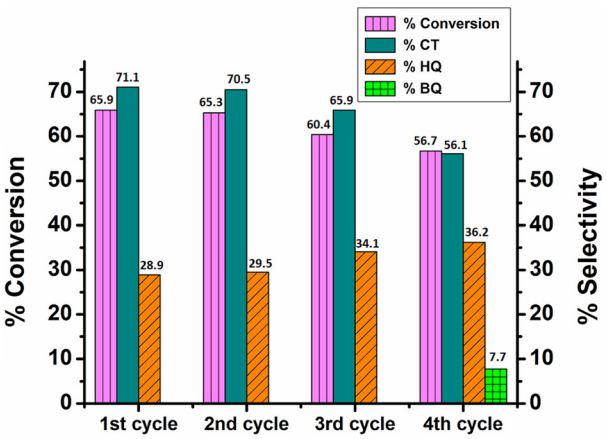

Fig. 20 Recyclability of compound **3** for the hydroxylation of phenol.

3.4.4 Heterogeneity test. A standard hot-filtration experiment was conducted under the respective optimized conditions catalyzed by the insoluble catalyst **3** to confirm the heterogeneous nature of the catalytic process and to exclude the possibility of potential homogeneous contributions. The solid catalyst **3** was separated from the reaction mixture at 45 min for styrene and at 1 h for phenol, after approximately

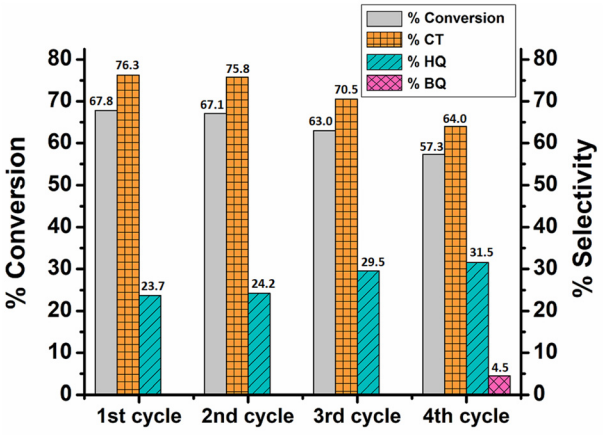

Fig. 21 Recyclability of compound 4 for the hydroxylation of phenol.

50% conversion was achieved for both the substrates (Fig. S13). The reactions were allowed to continue with the filtrate for an additional period of 3 h for styrene and 4 h for phenol using 3. No significant improvement in the conversion of styrene or phenol was observed after the separation of the catalyst, suggesting the true heterogeneous nature of the catalysts.

3.4.5 Utilization efficiency of H_2O_2. Assessment of the effective utilization of H_2O_2 or utilization efficiency of H_2O_2 in an oxidation reaction is important, as in general, transition metal catalysts tend to degrade H_2O_2 under higher reaction temperature conditions.[78] In the present study, the H_2O_2 efficiency percentage, which is defined as 100 × moles of H_2O_2 consumed in the formation of the oxidized product/moles of H_2O_2 converted[79] in phenol hydroxylation using 4 as a catalyst, was found to be 92.6%, which indeed is rather high in comparison with the values reported for many other phenol oxidation catalytic methodologies.[80,81] Furthermore, the utilization of H_2O_2 in styrene epoxidation using 4 as the catalyst was also found to be 81.2%. Considering that the epoxidation reaction was conducted at 80 °C for a longer period of 6 h under solvent-free conditions, the observed H_2O_2 efficiency in styrene epoxidation also appears to be reasonably good.

3.4.6 Comparison with some reported catalysts. An inspection of the comparative data listed in Table 5 revealed that the performances of the present homogeneous and heterogeneous CuO NP catalytic systems are significantly better than or comparable to those of most of the reported Cu-based catalytic epoxidation approaches, particularly with respect to parameters *viz*. conversion, selectivity, catalyst loading, and reaction conditions applied. As seen in Table 5, several existing reports on Cu-catalyzed epoxidation of styrene utilized TBHP as an oxidant,[23–25,61,82–87] with CH_3CN[66,71,82–84,87–92] or $CHCl_3$[85] as solvent. Whereas only two reports appear to be available on Cu-based catalysts in solvent-free styrene epoxidation, no reports were found related to styrene epoxidation catalyzed by CuO nano-catalysts under organic solventless conditions.[24,36] Furthermore, the present CuO nanocatalysts afforded competitive results in aqueous phase phenol hydroxylation to yield CT and HQ, in comparison with the activities of many other Cu based catalytic systems reported so far.[93–102] Overall, the optimized reaction conditions in both types of organic oxidations *viz*., styrene epoxidation and phenol hydroxylation in the present study are eco-friendly and milder as the reactions were carried out employing H_2O_2 as the oxygen source without the addition of organic solvent or any other non-green additives, at the natural pH of the reaction mixture attained.

3.4.7 Proposed catalytic cycle. The plausible catalytic cycles for styrene epoxidation and phenol hydroxylation are envisaged based on observations from our present work and previous literature.[103–105] As illustrated in Scheme 3, the oxidation

Table 5 The comparison of the activities of the catalysts 1, 2, 3 and 4 with various copper-based catalysts in the epoxidation of styrene

Entry	Catalyst	Catalyst amount	Conditions [time, temperature, oxidant, solvent]	Conversion (%)/ epoxide selectivity (%)	Ref.
1	**1**	0.002 mmol	6 h, 80 °C, 30% H_2O_2	98.5/99.0	This work
2	**2**	0.002 mmol	6 h, 80 °C, 30% H_2O_2	97.3/99.3	This work
3	**3**	1 mg	6 h, 80 °C, 30% H_2O_2	99.7/99.3	This work
4	**4**	1 mg	6 h, 80 °C, 30% H_2O_2	99.7/99.3	This work
5	$[Cu_2(\mu\text{-}O_2CC_6H_5)_4(py)_2]$	0.0065 mmol	25 h, RT, TBHP, solvent-free	78/82	24
6	CuO/In_2O_3	100 mg	3 h, reflux at 107 °C, anhydrous TBHP	65.2/73.7	61
7	$[Cu(tmbmz)_2]$	35 mg	6 h, 80 °C, 30% H_2O_2, CH_3CN	42.0/3.7	64
8	PS-$[Cu(ligand)_n]$	35 mg	6 h, 80 °C, 30% H_2O_2, CH_3CN	57.0/3.6	64
9	CuO CNCs@*meso*-SiO_2 nanocomposite	10 mg	2 h, 70 °C, TBHP, CH_3CN	88.6/61.2	82
10	[CuII(acpy-oap)Cl]-Y	35 mg	7 h, 80 °C, TBHP, CH_3CN	60.2/78.2	83
11	$[Cu(bipy)(5\text{-}Br\text{-}2\text{-}hap)(ClO_4)]_2$	2 mg	6 h, 60 °C, 30% H_2O_2, CH_3CN	100/58	91
12	CuO	7 mg	10 h, 70 °C, TBHP, CH_3CN	100/86.4 (% benzaldehyde)	23
13	$Cu(acac)_2$	50 mg	8 h, 80 °C, air, isobutyraldehyde, aq. NaOH, CH_3CN	28.6/18.5	66
14	[Cu(sal-dach)]-Y	25 mg	7 h, 80 °C, 30% H_2O_2, CH_3CN	21.7/12.9	89
15	Copper(II) Schiff base complex	0.032 mmol	6 h, refluxed, TBHP, $CHCl_3$	100/—	85
16	[Cu(sal-oaba) (H_2O)]-Y	25 mg	6 h, 80 °C, 30% H_2O_2, CH_3CN	23.4/15.8	90
17	$Fe_3O_4@SiO_2@[SB@Cu](CH_3COO)_2$	0.01 g	2 h, reflux, TBHP, CH_3OH	81.0/88.8	25

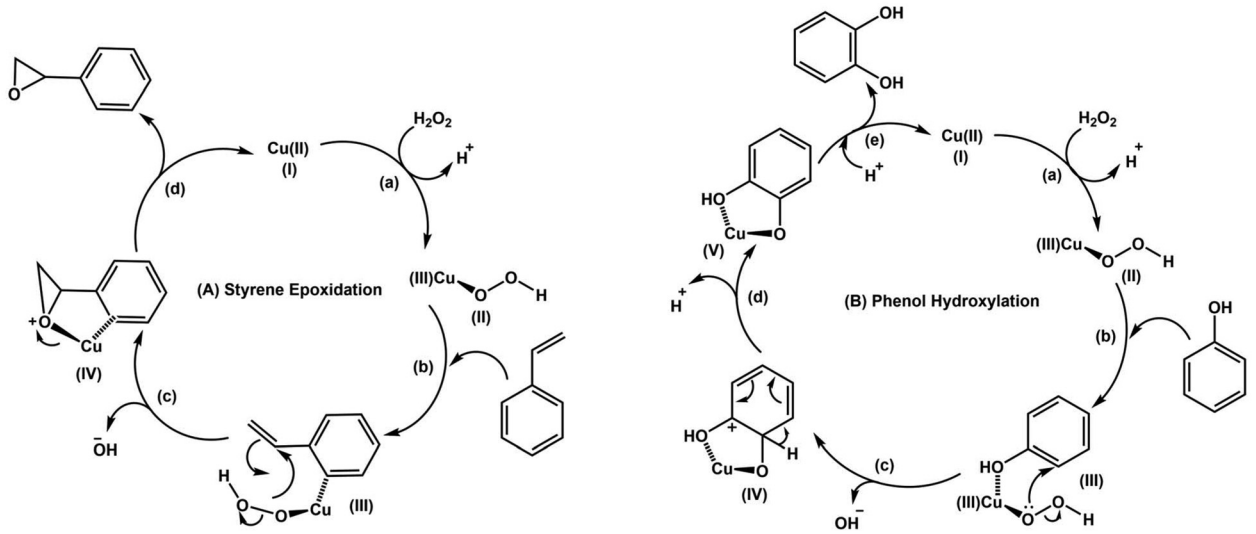

Scheme 3 Proposed catalytic cycle for (A) styrene epoxidation and (B) phenol hydroxylation. Cu–ligand coordination is not represented for clarity. Cu(II) represents the active Cu(II) center of complexes (**1** or **2**) or CuO nanomaterials (**3** or **4**).

processes for styrene and phenol proceed with the active Cu(II) metal center (I) of complexes (**1** or **2**) or the CuO nanomaterials (**3** or **4**) and lead to the formation of a Cu(III)–O–O–H (copper-hydroperoxide) intermediate (II) in the presence of H_2O_2 (reaction (a)).[104,106] The transfer of the coordinated oxygen atom from the Cu(III)–O–O–H intermediate initiates the formation of the oxidized products. In styrene epoxidation (A), the intermediate (II) forms an active species Cu-styrene-OOH^- (III) in the presence of styrene *via* interactions of H_2O_2 and the active Cu center (reaction (b)). The [Cu-styrene-OOH^-] species (III) facilitates the nucleophilic attack of the OOH^- species (reaction (c)) to form an intermediate (IV) and finally forms styrene epoxide (reaction (d)). Similarly, in phenol hydroxylation (B), a Cu-phenol-OOH^- intermediate is formed which leads to the nucleophilic attack of the OOH^- species at the *ortho* and *para* positions of the phenol molecule to produce hydroxylated CT and HQ; however the higher selectivity towards CT could be ascribed to the predominant interactions of the OOH^- species at the *ortho* position of phenol.[103,104]

4 Conclusions

In summary, our work highlights the successful application of the newly developed mixed ligand Cu(II) complexes with deferiprone and diimine co-ligands 2,2′-bipyridine and 1,10-phenanthroline as synthetic precursors for the straightforward synthesis of CuO nanosheets. These soluble complexes also served as versatile homogeneous catalysts in the epoxidation of styrene under solvent-free conditions as well as phenol hydroxylation in aqueous medium, respectively. Most importantly, the CuO NPs derived from compounds **1** and **2** could accomplish selective styrene epoxidation with impressive % conversions under solventless conditions. Furthermore, the same nanocatalysts displayed remarkable efficiency as water tolerant heterogeneous catalysts to facilitate phenol hydroxylation with H_2O_2 in aqueous medium. The nanocatalysts afford easy and successful regeneration and recyclability for at least three consecutive oxidation cycles. The sustainability of the developed oxidation protocols is further evident from the fact that apart from using a non-toxic metal catalyst and H_2O_2 as a standard green oxidant, the procedures are free from any halogenated solvents and acids or other hazardous auxiliaries. High utilization efficiency and a simple work-up procedure are other significant strengths of the methodologies making them economically and environmentally attractive.

Author contributions

Mitu Sharma – conceptualization, methodology, investigation, data collection, validation, formal analysis, and writing – original draft; Mukesh Sharma – methodology and investigation; Sazida Yasmin Sultana – review & editing; Mallayan Palaniandavar – conceptualization, review and editing; Nashreen S. Islam – supervision, funding acquisition, and writing – review and editing.

Conflicts of interest

There are no conflicts of interest to declare.

Data availability

Data will be made available on request.

Supplementary information is available. Supplementary information: characterization data for the complexes and the nanomaterials, reaction optimization data, characterization of

the regenerated catalysts, and heterogeneity test data. See DOI: https://doi.org/10.1039/d5dt01420d.

CCDC 1880241 and 1884417 contain the supplementary crystallographic data for this paper.[107a,b]

Acknowledgements

We are thankful to Dr Biraj Jyoti Borah, Department of Chemical Sciences, Tezpur University, Tezpur, Assam India, for helping us in solving the X-ray crystal structures.

References

1 H. Jayasimha, K. Chandrappa, P. Sanaulla and V. Dileepkumar, Green synthesis of CuO nanoparticles: A promising material for photocatalysis and electrochemical sensor, *Sens. Int.*, 2024, **5**, 100254.
2 C. L. Londoño-Calderón, P. Tancredi, S. Menchaca-Nal, N. J. Francois and L. G. Pampillo, Synergistic effects in magnetically recoverable nanocomposites of CuO nanoleaves with Fe3O4 nanoparticles for organic dye degradation, *Next Mater.*, 2025, **7**, 100370.
3 C. Wang, W. Zeng, T. Li and Y. Li, Hydrothermal synthesis of different CuO nano-flowers and their gas sensing property, *Mater. Technol.*, 2015, **30**(4), 205–212.
4 M.-J. Deng, C.-C. Wang, P.-J. Ho, C.-M. Lin, J.-M. Chen and K.-T. Lu, Facile electrochemical synthesis of 3D nanoarchitectured CuO electrodes for high-performance supercapacitors, *J. Mater. Chem. A*, 2014, **2**(32), 12857–12865.
5 T. Umegaki, Y. Kojima and K. Omata, Effect of oxide coating on performance of copper-zinc oxide-based catalyst for methanol synthesis via hydrogenation of carbon dioxide, *Materials*, 2015, **8**(11), 7738–7744.
6 K. Cao, H. Liu, W. Li, Q. Han, Z. Zhang, K. Huang, Q. Jing and L. Jiao, CuO nanoplates for high–performance potassium–ion batteries, *Small*, 2019, **15**(36), 1901775.
7 O. Perlman, I. S. Weitz and H. Azhari, Copper oxide nanoparticles as contrast agents for MRI and ultrasound dual-modality imaging, *Phys. Med. Biol.*, 2015, **60**(15), 5767.
8 V. Gnanavel, V. Palanichamy and S. M. Roopan, Biosynthesis and characterization of copper oxide nanoparticles and its anticancer activity on human colon cancer cell lines (HCT-116), *J. Photochem. Photobiol., B*, 2017, **171**, 133–138.
9 A. Kalaiarasi, R. Sankar, C. Anusha, K. Saravanan, K. Aarthy, S. Karthic, T. l. Mathuram and V. Ravikumar, Copper oxide nanoparticles induce anticancer activity in A549 lung cancer cells by inhibition of histone deacetylase, *Biotechnol. Lett.*, 2018, **40**, 249–256.
10 W. Wang, P. Gao, H. Gui, X. Wei, H. Zhang and X. Wang, Copper-based nanomaterials for the treatment of bacteria-infected wounds: material classification, strategies and mechanisms, *Coord. Chem. Rev.*, 2025, **522**, 216205.
11 W. Mohsen, M. Sadek and H. A. Elazab, *Green synthesis of copper oxide nanoparticles in aqueous medium as a potential efficient catalyst for catalysis applications*. 2017.
12 J. Singh, G. Kaur and M. Rawat, A brief review on synthesis and characterization of copper oxide nanoparticles and its applications, *J. Bioelectron. Nanotechnol.*, 2016, **1**(1), 9.
13 G. Qiu, S. Dharmarathna, Y. Zhang, N. Opembe, H. Huang and S. L. Suib, Facile microwave-assisted hydrothermal synthesis of CuO nanomaterials and their catalytic and electrochemical properties, *J. Phys. Chem. C*, 2012, **116**(1), 468–477.
14 M. Aghayan, I. Hussainova, K. Kirakosyan and M. A. Rodríguez, The template-assisted wet-combustion synthesis of copper oxide nanoparticles on mesoporous network of alumina nanofibers, *Mater. Chem. Phys.*, 2017, **192**, 138–146.
15 V. V. Kumar, A. Dharani, M. Mariappan and S. P. Anthony, Synthesis of CuO and Cu 2 O nano/microparticles from a single precursor: Effect of temperature on CuO/Cu 2 O formation and morphology dependent nitroarene reduction, *RSC Adv.*, 2016, **6**(88), 85083–85090.
16 W.-H. Pi, Q.-J. Li, M. Wu, Y.-Z. Huang, X.-L. Deng, L. Huang, L.-B. Jiang and H.-X. Zhang, Utilization of a dicopper(II) complex of tetrapyridyl ligand as the precursor for the synthesis of copper-based composites and their catalysis, *Appl. Surf. Sci.*, 2019, **493**, 185–192.
17 A. M. A. Adam, A. Alhadhrami, H. A. Saad and M. S. Refat, Synthesis and spectroscopic characterizations of Cu(II) complexes with novel 15-membered N4 macrocyclic ligand and their utility to obtain CuO nanostructures for efficient degradation of dyes, *Appl. Organomet. Chem.*, 2018, **32**(1), e3950.
18 M. Y. Nassar, H. M. Aly, M. E. Moustafa and E. A. Abdelrahman, Synthesis, characterization and biological activity of new 3-substitued-4-amino-5-hydrazino-1, 2, 4-triazole schiff bases and their Cu(II) complexes: a new approach to CuO nanoparticles for photocatalytic degradation of methylene blue dye, *J. Inorg. Organomet. Polym. Mater.*, 2017, **27**, 1220–1233.
19 P. Selvam, S. Sathiyakumar, K. Srinivasan and T. Premkumar, A Copper(II) complex of a new hydrazone: A solid-state single source precursor for the preparation of both Cu and CuO nanoparticles, *J. Mol. Struct.*, 2019, 469–475.
20 S. Y. Ebrahimipour, I. Sheikhshoaie, J. Castro, W. Haase, M. Mohamadi, S. Foro, M. Sheikhshoaie and S. Esmaeili-Mahani, A novel cationic copper(II) Schiff base complex: Synthesis, characterization, crystal structure, electrochemical evaluation, anti-cancer activity, and preparation of its metal oxide nanoparticles, *Inorg. Chim. Acta*, 2015, **430**, 245–252.
21 R. Poreddy, C. Engelbrekt and A. Riisager, Copper oxide as efficient catalyst for oxidative dehydrogenation of alcohols with air, *Catal. Sci. Technol.*, 2015, **5**(4), 2467–2477.
22 M. Lashanizadegan and N. Erfaninia, Synthesis, characterization and catalytic property of CuO and Ag/CuO nano-

particles for the epoxidation of styrene, *Korean J. Chem. Eng.*, 2013, **30**, 2007–2011.

23 D. Ge, J. Wang, H. Geng, S. Lu, D. Wang, X. Li, X. Zhao, X. Cao and H. Gu, Facile Synthesis of Copper–Based Metal Oxide Nanoparticles with Exceptional Catalytic Activity for the Selective Oxidation of Styrenes into Benzaldehydes, *ChemPlusChem*, 2015, **80**(3), 511–515.

24 Z. Islam, P. K. Kouli, S. Baruah, M. Chakrabortty, R. A. Bepari and B. K. Das, Dimeric copper(II) tetracarboxylates as catalysts in the selective epoxidation of styrene, *Polyhedron*, 2018, **155**, 351–358.

25 S. Panahandehjo, M. Lashanizadegan, K. Mohammadi and M. Zahedi-Tabrizi, New Cu(II) Schiff-base complex modified on magnetic nanoparticles: Oxidation and DFT investigation, *J. Mol. Struct.*, 2024, **1308**, 138086.

26 X. Song, L. Yang, X. Chang, S. Miao and H. Zhang, Synthesis of NaLTA zeolite confined CuO catalysts and superior catalytic properties for alkene epoxidation with H_2O_2 as oxidant, *Inorg. Chem. Commun.*, 2024, 113453.

27 L. Wu and B. Li, Efficient epoxidation of styrene over single-atomic copper-doped ordered mesoporous alumina (Cu-OMA) composited with carbon nitride, *J. Mol. Struct.*, 2025, 140050.

28 G. Saikia, K. Ahmed, C. Rajkhowa, M. Sharma, H. Talukdar and N. S. Islam, Polymer immobilized tantalum(v)–amino acid complexes as selective and recyclable heterogeneous catalysts for oxidation of olefins and sulfides with aqueous H 2 O 2, *New J. Chem.*, 2019, **43**(44), 17251–17266.

29 S. Y. Sultana, M. Sharma, H. Talukdar, T. Begum, N. K. Gour, B. Sarma and N. S. Islam, New mixed ligand oxido-vanadium(v) complexes with O, O-donor and diimine ligands: Synthesis, crystal structure and catalytic activity in eco-friendly oxidation of olefins and phenol, *Mol. Catal.*, 2024, **565**, 114352.

30 K. Ahmed, G. Saikia, S. Paul, S. D. Baruah, H. Talukdar, M. Sharma and N. S. Islam, Water-soluble polymer anchored peroxotitanates as environmentally clean and recyclable catalysts for mild and selective oxidation of sulfides with H_2O_2 in water, *Tetrahedron*, 2019, **75**(44), 130605.

31 G. Saikia, K. Ahmed, S. R. Gogoi, M. Sharma, H. Talukdar and N. S. Islam, A chitosan supported peroxidovanadium (v) complex: Synthesis, characterization and application as an eco-compatible heterogeneous catalyst for selective sulfoxidation in water, *Polyhedron*, 2019, **159**, 192–205.

32 J. J. Boruah, K. Ahmed, S. Das, S. R. Gogoi, G. Saikia, M. Sharma and N. S. Islam, Peroxomolybdate supported on water soluble polymers as efficient catalysts for green and selective sulfoxidation in aqueous medium, *J. Mol. Catal. A: Chem.*, 2016, **425**, 21–30.

33 M. Sharma, G. Saikia, K. Ahmed, S. R. Gogoi, V. G. Puranik and N. S. Islam, Vanadium-based polyoxometalate complex as a new and efficient catalyst for phenol hydroxylation under mild conditions, *New J. Chem.*, 2018, **42**(7), 5142–5152.

34 S. Baruah and A. Puzari, Development of a new methodology for the synthesis of chloro (glycinato) 1, 10-phenanthroline copper(II) monohydrate and analogous complexes and study of their catalytic utility towards selective hydroxylation of phenol, *Inorg. Nano-Met. Chem.*, 2017, **47**(11), 1542–1547.

35 L. Zou, M. Zhu, J. Liu, L. Chen, Q. Yao, N. Hu, X. Chen and H. Kita, Preparation and characterization of high catalytic performance supported TS-2 zeolites for phenol hydroxylation, *Microporous Mesoporous Mater.*, 2024, **363**, 112823.

36 R. Sadasivan, A. Patel and A. Ballabh, Investigation of catalytic properties of Cs salt of di-copper substituted phosphotungstate, Cs7 [PW10Cu2 (H_2O) O38] in epoxidation of styrene, *Inorg. Chim. Acta*, 2019, **487**, 345–353.

37 F. Delavar Mendi, A. Sh. Saljooghi, M. Ramezani, R. Kruszynski, M. Poupon, M. Kucerakova, V. Huch, P. Socha, M. Babaei and M. Alibolandi, Five new complexes with deferiprone and N, N-donor ligands: evaluation of cytotoxicity against breast cancer MCF-7 cell line and HSA-binding determination, *J. Biomol. Struct. Dyn.*, 2021, **39**(13), 4845–4858.

38 D.-H. Zou, M. Liang and W. Chen, Synthesis, X-Ray Crystal Structures and, Catalytic Epoxidation of Oxidovanadium (v) Complexes with Aroylhydrazone and Ethyl Maltolate Ligands, *Acta Chim. Slov.*, 2021, **68**(2), 441–446.

39 S. Y. Sultana, H. Talukdar, B. J. Borah, M. Sharma and N. S. Islam, Synthesis, structure and catalytic activity of new oxovanadium(v) complexes with deferiprone and N, N-donor ligands, *Inorg. Chim. Acta*, 2022, **534**, 120813.

40 S. Kaviani, M. Izadyar and M. R. Housaindokht, A DFT study on the metal ion selectivity of deferiprone complexes, *Comput. Biol. Chem.*, 2020, **86**, 107267.

41 A. Irto, F. Crea, M. Milone, G. Gattuso, C. Bretti, C. De Stefano and R. M. Cigala, Deferiprone: new environmental perspectives. Insights into its sequestering ability vs. different metal cations, *Ecotoxicol. Environ. Saf.*, 2024, **272**, 116027.

42 S. Iranpour, K. Abnous, S. M. Taghdisi and A. S. Saljooghi, Towards the preparation of smart drug delivery platforms for colorectal cancer therapy: Biocompatible and targeted mesoporous silica nanoparticles with the deferiprone-copper complex gatekeeper, *J. Drug Delivery Sci. Technol.*, 2024, **100**, 106087.

43 G. M. Sheldrick, A short history of SHELX, *Acta Crystallogr., Sect. A: Found. Crystallogr.*, 2008, **64**(1), 112–122.

44 M. N. Burnett and C. K. Johnson, ORTEP-III: Oak Ridge thermal ellipsoid plot program for crystal structure illustrations. Oak ridge national laboratory report ORNL-6895, Oak Ridge, Tennessee: 1996.

45 A. Barve, A. Kumbhar, M. Bhat, B. Joshi, R. Butcher, U. Sonawane and R. Joshi, Mixed-ligand copper(II) maltolate complexes: synthesis, characterization, DNA binding and cleavage, and cytotoxicity, *Inorg. Chem.*, 2009, **48**(19), 9120–9132.

46 B. Selvakumar, V. Rajendiran, P. U. Maheswari, H. Stoeckli-Evans and M. Palaniandavar, Structures, spectra, and DNA-binding properties of mixed ligand copper(II) complexes of iminodiacetic acid: The novel role of diimine co-ligands on DNA conformation and hydrolytic and oxidative double strand DNA cleavage, *J. Inorg. Biochem.*, 2006, **100**(3), 316–330.
47 R. Loganathan, M. Ganeshpandian, N. S. Bhuvanesh, M. Palaniandavar, A. Muruganantham, S. K. Ghosh, A. Riyasdeen and M. A. Akbarsha, DNA and protein binding, double-strand DNA cleavage and cytotoxicity of mixed ligand copper(II) complexes of the antibacterial drug nalidixic acid, *J. Inorg. Biochem.*, 2017, **174**, 1–13.
48 J. E. Huheey, E. A. Keiter, R. L. Keiter and O. K. Medhi, *Inorganic chemistry: principles of structure and reactivity*, Pearson Education India, 2006.
49 G. Murphy, C. Murphy, B. Murphy and B. Hathaway, Comparative crystallography. 4. Crystal structures, electronic properties and structural pathways of two [Cu (phen)(2)(OH2)][Y], complexes (phen equals 1, 10-phenanthroline, Y = CF3SO3-or ClO4-), *J. Chem. Soc., Dalton Trans.*, 1997, **15**, 2653–2660.
50 P. T. Selvi, M. Murali, M. Palaniandavar, M. Köckerling and G. Henkel, X-ray crystal structure of tetrakis (1-methylcytosine) copper(II) perchlorate dihydrate: effect of 1-methyl substitution on cytosine on the spectral and redox behaviour, *Inorg. Chim. Acta*, 2002, **340**, 139–146.
51 V. Rajendiran, R. Karthik, M. Palaniandavar, H. Stoeckli-Evans, V. S. Periasamy, M. A. Akbarsha, B. S. Srinag and H. Krishnamurthy, Mixed-ligand copper(II)-phenolate complexes: effect of coligand on enhanced DNA and protein binding, DNA cleavage, and anticancer activity, *Inorg. Chem.*, 2007, **46**(20), 8208–8221.
52 R. Loganathan, S. Ramakrishnan, E. Suresh, M. Palaniandavar, A. Riyasdeen and M. A. Akbarsha, Mixed ligand μ-phenoxo-bridged dinuclear copper(II) complexes with diimine co-ligands: efficient chemical nuclease and protease activities and cytotoxicity, *Dalton Trans.*, 2014, **43**(16), 6177–6194.
53 A. Paulovicova, U. El-Ayaan and Y. Fukuda, Synthesis, characterization and X-ray crystal structures of two five-coordinate ternary copper(II) complexes containing acetylacetonate with 1, 10-phenanthroline and 2, 9-dimethyl phenanthroline, *Inorg. Chim. Acta*, 2001, **321**(1–2), 56–62.
54 T. Ajaykamal, M. Köckerling and M. Palaniandavar, Copper(II)-flavonolate complexes of 2N ligands as functional models for quercetin 2, 4-dioxygenase enzymes: The role of axially coordinated water and ligand substitution on dioxygenase activity, *Inorg. Chim. Acta*, 2023, **556**, 121673.
55 S. Thanneeru, S. S. Duay, L. Jin, Y. Fu, A. M. Angeles-Boza and J. He, Single chain polymeric nanoparticles to promote selective hydroxylation reactions of phenol catalyzed by copper, *ACS Macro Lett.*, 2017, **6**(7), 652–656.
56 M. Ahamed, H. A. Alhadlaq, M. M. Khan, P. Karuppiah and N. A. Al-Dhabi, Synthesis, characterization, and antimicrobial activity of copper oxide nanoparticles, *J. Nanomater.*, 2014, **2014**(1), 637858.
57 S. Pansambal, K. Deshmukh, A. Savale, S. Ghotekar, O. Pardeshi, G. Jain, Y. Aher and D. Pore, Phytosynthesis and biological activities of fluorescent CuO nanoparticles using Acanthospermum hispidum L, extract, *J. Nanostruct.*, 2017, **7**(3), 165–174.
58 L. Arfaoui, F. Janene, S. Kouass, S. Mignard, F. Touati and H. Dhaouadi, CuO nanosheets: synthesis, characterization, and catalytic performance, *Russ. J. Inorg. Chem.*, 2019, **64**(13), 1687–1696.
59 A. S. Ethiraj and D. J. Kang, Synthesis and characterization of CuO nanowires by a simple wet chemical method, *Nanoscale Res. Lett.*, 2012, **7**, 1–5.
60 M. Qian, X. Liu, S. Cui, H. Jia and P. Du, Copper oxide nanosheets prepared by molten salt method for efficient electrocatalytic oxygen evolution reaction with low catalyst loading, *Electrochim. Acta*, 2018, **263**, 318–327.
61 V. R. Choudhary, R. Jha, N. K. Chaudhari and P. Jana, Supported copper oxide as a highly active/selective catalyst for the epoxidation of styrene by TBHP to styrene oxide, *Catal. Commun.*, 2007, **8**(10), 1556–1560.
62 E. Kamaraj, S. Somasundaram, K. Balasubramani, M. P. Eswaran, R. Muthuramalingam and S. Park, Facile fabrication of CuO-Pb2O3 nanophotocatalyst for efficient degradation of Rose Bengal dye under visible light irradiation, *Appl. Surf. Sci.*, 2018, **433**, 206–212.
63 A. El-Trass, H. ElShamy, I. El-Mehasseb and M. El-Kemary, CuO nanoparticles: synthesis, characterization, optical properties and interaction with amino acids, *Appl. Surf. Sci.*, 2012, **258**(7), 2997–3001.
64 P. K. Raul, S. Senapati, A. K. Sahoo, I. M. Umlong, R. R. Devi, A. J. Thakur and V. Veer, CuO nanorods: a potential and efficient adsorbent in water purification, *RSC Adv.*, 2014, **4**(76), 40580–40587.
65 X. Qiu, M. Miyauchi, H. Yu, H. Irie and K. Hashimoto, Visible-Light-Driven Cu(II)–(Sr1− y Na y)(Ti1− x Mo x) O3 Photocatalysts Based on Conduction Band Control and Surface Ion Modification, *J. Am. Chem. Soc.*, 2010, **132**(43), 15259–15267.
66 X. Wang, S. Wu, Z. Li, X. Yang, J. Hu, Q. Huo, J. Guan and Q. Kan, Oxovanadium(IV), copper(II) or cobalt(II) acetylacetone complexes immobilized on amino–functionalized CMK–3 for the aerobic epoxidation of styrene, *Appl. Organomet. Chem.*, 2015, **29**(10), 698–706.
67 M. Kamali, F. Samari and F. Sedaghati, Low-temperature phyto-synthesis of copper oxide nanosheets: Its catalytic effect and application for colorimetric sensing, *Mater. Sci. Eng., C*, 2019, **103**, 109744.
68 F. Zhang, A. Zhu, Y. Luo, Y. Tian, J. Yang and Y. Qin, CuO nanosheets for sensitive and selective determination of H_2S with high recovery ability, *J. Phys. Chem. C*, 2010, **114**(45), 19214–19219.
69 K. Sing, *Adsorption, surface area, and porosity*, Academic Press, 1967.

70 Z. Tian, H. Bai, Y. Li, W. Liu, J. Li, Q. Kong and G. Xi, Gas–Sensing Activity of Amorphous Copper Oxide Porous Nanosheets, *ChemistryOpen*, 2020, **9**(1), 80–86.
71 C. Tamuly, I. Saikia, M. Hazarika and M. R. Das, Bio-derived CuO nanocatalyst for oxidation of aldehyde: a greener approach, *RSC Adv.*, 2014, **4**(40), 20636–20640.
72 A. F. Zedan, A. T. Mohamed, M. S. El-Shall, S. Y. AlQaradawi and A. S. AlJaber, Tailoring the reducibility and catalytic activity of CuO nanoparticles for low temperature CO oxidation, *RSC Adv.*, 2018, **8**(35), 19499–19511.
73 K. Tanaka and F. Toda, Solvent-free organic synthesis, *Chem. Rev.*, 2000, **100**(3), 1025–1074.
74 K. N. Bhagya and V. Gayathri, Metal complexes of 2-methylimidazole encapsulated in zeolite-Y as efficient and reusable catalysts for oxidation of phenol and benzyl alcohol, *J. Porous Mater.*, 2013, **20**, 257–266.
75 M. R. Maurya and S. Sikarwar, Oxidation of phenol and hydroquinone catalysed by copper(II) and oxovanadium(IV) complexes of N, N′-bis (salicyledene) diethylenetriamine (H_2saldien) covalently bonded to chloromethylated polystyrene, *J. Mol. Catal. A: Chem.*, 2007, **263**(1–2), 175–185.
76 S. Narayan, J. Muldoon, M. Finn, V. V. Fokin, H. C. Kolb and K. B. Sharpless, "On water": unique reactivity of organic compounds in aqueous suspension, *Angew. Chem.*, 2005, **117**(21), 3339–3343.
77 X.-Y. Shi and J.-F. Wei, Selective oxidation of sulfide catalyzed by peroxotungstate immobilized on ionic liquid-modified silica with aqueous hydrogen peroxide, *J. Mol. Catal. A: Chem.*, 2008, **280**(1–2), 142–147.
78 P. J. Cordeiro and T. D. Tilley, Enhancement of epoxidation efficiencies for Ta-SBA15 catalysts. The influence of modification with–EMe3 (E = Si, Ge, Sn) groups, *Langmuir*, 2011, **27**(10), 6295–6304.
79 V. Hulea, A.-L. Maciuca, F. Fajula and E. Dumitriu, Catalytic oxidation of thiophenes and thioethers with hydrogen peroxide in the presence of W-containing layered double hydroxides, *Appl. Catal., A*, 2006, **313**(2), 200–207.
80 N. Inchaurrondo, P. Massa, R. Fenoglio, J. Font and P. Haure, Efficient catalytic wet peroxide oxidation of phenol at moderate temperature using a high-load supported copper catalyst, *Chem. Eng. J.*, 2012, **198**, 426–434.
81 D. R. Godhani, H. D. Nakum, D. K. Parmar, J. P. Mehta and N. C. Desai, A hierarchical zeolite-Y hampered metallo-ligand complexes for selective oxidation: A mechanistic point of view, *Microporous Mesoporous Mater.*, 2016, **235**, 233–245.
82 C. Chen, J. Qu, C. Cao, F. Niu and W. Song, CuO nanoclusters coated with mesoporous SiO 2 as highly active and stable catalysts for olefin epoxidation, *J. Mater. Chem.*, 2011, **21**(15), 5774–5779.
83 M. R. Maurya, P. Saini, C. Haldar, A. K. Chandrakar and S. Chand, Oxidation of styrene and cyclohexene with TBHP catalyzed by copper(II) complex encapsulated in zeolite-Y, *J. Coord. Chem.*, 2012, **65**(16), 2903–2918.
84 W. Jia, Y. Liu, P. Hu, R. Yu, Y. Wang, L. Ma, D. Wang and Y. Li, Ultrathin CuO nanorods: controllable synthesis and superior catalytic properties in styrene epoxidation, *Chem. Commun.*, 2015, **51**(42), 8817–8820.
85 F. Heshmatpour, S. Rayati, M. A. Hajiabbas, P. Abdolalian and B. Neumüller, Copper(II), Schiff base complexes derived from 2, 2′-dimethyl-propandiamine: Synthesis, characterization and catalytic performance in the oxidation of styrene and cyclooctene, *Polyhedron*, 2012, **31**(1), 443–450.
86 M. Pourshahi, Y. Mansoori, F. Ghahramani, A. Bezaatpour, D. Esquivel, M. A. Navarro and M. John, Copper(II)-polymer chelate grafted from magnetic mesoporous silica for the O-arylation of phenols via the Ullmann reaction, *J. Organomet. Chem.*, 2024, **1014**, 123191.
87 Y. Fu, L. Liu, S. Tricard, K. Liang, J. Zhang, J. Fang and J. Zhao, Slow pyrolysis of Cu/Co-Co Prussian blue analog to enhance catalytic activity and selectivity in epoxidation of styrene, *Appl. Catal., A*, 2023, **657**, 119161.
88 M. R. Maurya, A. Arya, P. Adao and J. C. Pessoa, Immobilisation of oxovanadium(IV), dioxomolybdenum(VI) and copper(II) complexes on polymers for the oxidation of styrene, cyclohexene and ethylbenzene, *Appl. Catal., A*, 2008, **351**(2), 239–252.
89 M. R. Maurya, A. K. Chandrakar and S. Chand, Oxovanadium(IV) and copper(II) complexes of 1, 2-diaminocyclohexane based ligand encapsulated in zeolite-Y for the catalytic oxidation of styrene, cyclohexene and cyclohexane, *J. Mol. Catal. A: Chem.*, 2007, **270**(1–2), 225–235.
90 M. R. Maurya, A. K. Chandrakar and S. Chand, Zeolite-Y encapsulated metal complexes of oxovanadium(VI), copper (II) and nickel(II) as catalyst for the oxidation of styrene, cyclohexane and methyl phenyl sulfide, *J. Mol. Catal. A: Chem.*, 2007, **274**(1–2), 192–201.
91 S. Shit, U. Yadava, D. Saha and R. Fröhlich, 2, 2′-Bipyridyl-acetylphenolato mixed ligand copper(II) complexes: syntheses, characterizations and catalytic activity in styrene epoxidation, *J. Coord. Chem.*, 2013, **66**(1), 66–76.
92 B. Shi, H. Yu, S. Gao, L. Zhang, Y. Liu and K. Huang, Copper complex supported on hollow porous nanosphere frameworks with improved catalytic activity for epoxidation of olefins, *Microporous Mesoporous Mater.*, 2020, **294**, 109890.
93 G. Shi, Y. Bao, B. Chen and J. Xu, Phenol hydroxylation over cubic/monoclinic mixed phase CuO nanoparticles prepared by chemical vapor deposition, *React. Kinet., Mech. Catal.*, 2017, **122**, 289–303.
94 Y.-Y. Huang, H. Konnerth, J.-Y. Yeh, M. H. Prechtl, C.-Y. Wen and K. C.-W. Wu, De novo synthesis of Cr-embedded MOF-199 and derived porous CuO/CuCr 2 O 4 composites for enhanced phenol hydroxylation, *Green Chem.*, 2019, **21**(8), 1889–1894.
95 H. Wang, J. Hu, Z. Wu, F. Shi and L. Zhang, Preparation of a 2, 2′-(4-nitrophenyl) dipyrromethane copper coordination compound and its catalytic behavior for phenol

hydroxylation, *React. Kinet., Mech. Catal.*, 2014, **111**, 697–707.

96 W. Du, J. Pang, J. Ma, W. Wang and L. Zhang, Preparation of graphene supported copper composite materials and study on the catalytic activity of phenol hydroxylation, *Mater. Today Sustainability*, 2024, **26**, 100714.

97 S. Kannan, A. Dubey and H. Knozinger, Synthesis and characterization of CuMgAl ternary hydrotalcites as catalysts for the hydroxylation of phenol, *J. Catal.*, 2005, **231**(2), 381–392.

98 A. L. Villa, C. A. Caro and C. M. de Correa, Cu-and Fe-ZSM-5 as catalysts for phenol hydroxylation, *J. Mol. Catal. A: Chem.*, 2005, **228**(1–2), 233–240.

99 M. R. Maurya, A. K. Chandrakar and S. Chand, Oxidation of phenol, styrene and methyl phenyl sulfide with H_2O_2 catalysed by dioxovanadium(v) and copper(ii) complexes of 2-aminomethylbenzimidazole-based ligand encapsulated in zeolite-Y, *J. Mol. Catal. A: Chem.*, 2007, **263**(1–2), 227–237.

100 K. Anjali, V. Ganesh, J. Christopher and A. Sakthivel, Copper based macromolecular catalysts for the hydroxylation of phenols, *J. Organomet. Chem.*, 2020, **929**, 121579.

101 F. Shi, Y. Chen, L. Sun, L. Zhang and J. Hu, Hydroxylation of phenol catalyzed by different forms of Cu–alginate with hydrogen peroxide as an oxidant, *Catal. Commun.*, 2012, **25**, 102–105.

102 O. Amadine, Y. Essamlali, A. Fihri, M. Larzek and M. Zahouily, Effect of calcination temperature on the structure and catalytic performance of copper–ceria mixed oxide catalysts in phenol hydroxylation, *RSC Adv.*, 2017, **7**(21), 12586–12597.

103 E. Naranov, D. Ramazanov, M. Agliullin, O. Sinyashin and A. Maximov, Recent Advances in Aromatic Hydroxylation to Phenol and Hydroquinone Using H_2O_2, *Catalysts*, 2024, **14**(12), 930.

104 E. Shilpa and V. Gayathri, Encapsulation of Cu(ii)[2-(2′-hydroxyphenyl) benzimidazole] 2 within zeolite nanocavity: structural properties and its catalytic activity towards phenol and styrene oxidation, *J. Environ. Chem. Eng.*, 2016, **4**(4), 4194–4206.

105 M. S. Batra, R. Dwivedi and R. Prasad, Recent developments in heterogeneous catalyzed epoxidation of styrene to styrene oxide, *ChemistrySelect*, 2019, **4**(40), 11636–11673.

106 M. R. Maurya, M. Kumar and U. Kumar, Polymer-anchored vanadium(iv), molybdenum(vi) and copper(ii) complexes of bidentate ligand as catalyst for the liquid phase oxidation of organic substrates, *J. Mol. Catal. A: Chem.*, 2007, **273**(1–2), 133–143.

107 (*a*) M. Sharma, M. Sharma, S. Y. Sultana, M. Palaniandavar and N. S. Islam, CCDC 1880241: Experimental Crystal Structure Determination, 2025, DOI: **10.5517/ccdc.csd.cc213jyn**; (*b*) M. Sharma, M. Sharma, S. Y. Sultana, M. Palaniandavar and N. S. Islam, CCDC 1884417: Experimental Crystal Structure Determination, 2025, DOI: **10.5517/ccdc.csd.cc217wnv**.